

Supplementary Information for Triple Hydrogen Atom Abstraction from Mn-NH₃ Complexes Results in Cyclophosphazenum Cations

Brian J. Cook, Samantha I. Johnson, Geoffrey M. Chambers, Werner Kaminsky, and R. Morris Bullock*

Experimental	S5
Computational Details	S6
Scheme S1. Pathway for free dihydrophosphazenum reacting with ArO• radical. All free energies in kcal/mol.....	S6
Table S1. Spin State and Relative Energies for Computationally Determined Species.	S6
Synthesis of New Complexes:.....	S7
Crystallographic Details.....	S11
Table S2: Crystallographic data for 1.	S12
Table S3. Crystallographic data for 2	S14
Table S4: Crystallographic data for 3.	S16
Table S5: Crystallographic data for 4.	S18
Table S6: Crystallographic data for [Mn(dppe) ₂ (CO) ₂]BAr ^F ₄	S20
Figure S1. Space-filling diagram comparing 2 (left) and 1 (right).	S21
Figure S2. ORTEP representation of the cation-anion pair of 1.....	S21
Figure S3. ORTEP representation of the cation-anion pair for 2.	S22
Figure S4. ORTEP representation of cation-anion pair of 3. Hydrogen atoms and lattice guests have been removed for clarity.	S22
Figure S5. ORTEP representation (50% ellipsoid probability) of 4 Hydrogen atoms have been removed for clarity.	S23
Figure S6. ORTEP representation of [Mn(dppe) ₂ (CO) ₂]BAr ^F ₄ , isolated from the same reaction mixture along with 4.	S23
Figure S7. ¹ H NMR spectrum of 1 in PhF.	S24
Figure S8. ¹ H NMR spectrum of 1- ¹⁵ N in PhF.	S24
Figure S9. ³¹ P{ ¹ H} NMR spectrum of 1 in PhF after crystallization and isolation.	S25
Figure S10. FT-IR spectrum of 1 in CH ₂ Cl ₂ , with background signal subtracted.	S25
Figure S11. ³¹ P{ ¹ H} NMR spectrum of [Mn(depe) ₂ (CO)]B(C ₆ F ₅) ₄ before (top) and after (bottom) addition of NH ₃ in PhF.	S26
Figure S12. ³¹ P{ ¹ H} NMR spectrum of as-synthesized 1- ¹⁵ N in PhF.	S26
Figure S13. ¹⁵ N{ ¹ H} NMR spectrum of 1- ¹⁵ N in PhF.	S27

Figure S14. ^1H NMR spectrum of $2^+\text{B}(\text{C}_6\text{F}_5)_4^-$ in CDCl_3 . * denotes solvent-derived impurities.....	S27
Figure S15. ^1H NMR spectrum recorded in PhF of $2\text{-}^{15}\text{N}$. Inset shows an expansion of the NH_3 signal and coupling. * denotes solvent-derived impurities.	S28
Figure S16. ^1H NMR spectrum of $2\text{-}^{15}\text{N}$ in CDCl_3 . * denotes solvent-derived impurities.	S28
Figure S17. $^{31}\text{P}\{^1\text{H}\}$ NMR spectrum of 2 in PhF.	S29
Figure S18. $^{31}\text{P}\{^1\text{H}\}$ NMR spectrum in PhF of as-synthesized $2\text{-}^{15}\text{N}$	S29
Figure S19. $^{13}\text{C}\{^1\text{H}\}$ NMR spectrum of $2\text{-}^{15}\text{N}$ in CDCl_3	S30
Figure S20. $^{15}\text{N}\{^1\text{H}\}$ NMR spectrum of $2\text{-}^{15}\text{N}$ in PhF.	S30
Figure S21. ^{19}F NMR spectrum of $2\text{-}^{15}\text{N}$ in CDCl_3	S31
Figure S22. FT-IR spectrum of 2 in CH_2Cl_2 , with background solvent signals subtracted.	S31
Figure S23. $^{31}\text{P}\{^1\text{H}\}$ NMR spectrum of as-synthesized $5\text{-}^{15}\text{N}$ in PhF.	S32
Figure S24. $^{31}\text{P}\{^1\text{H}\}$ NMR spectrum of $[\text{Mn}(\text{dppp})(\text{dppm})(\text{CO})]\text{BAr}^{\text{F}}_4$ before (bottom) and after (top) NH_3 addition.	S32
Figure S25. ^1H NMR spectrum of $5\text{-}^{15}\text{N}$ in situ after addition of $^{15}\text{NH}_3$	S33
Figure S26. $^{31}\text{P}\{^1\text{H}\}$ NMR spectrum of the reaction between $5\text{-}^{15}\text{N}$ before (red) and after (blue) and 3.0 equiv. ArO^\bullet in PhF.	S33
Figure S27. ^1H NMR spectrum of the reaction between $5\text{-}^{15}\text{N}$ and 3.0 equiv. ArO^\bullet recorded in PhF.	S34
Figure S28. ^1H NMR spectrum in CDCl_3 of 3 isolated after crystallization from the reaction of 1 and 3.0 equiv. ArO^\bullet	S34
Figure S29. FT-IR spectrum of the reaction between 1 and 3 equiv. ArO^\bullet recorded in CH_2Cl_2 . Background solvent signals have been subtracted.	S35
Figure S30. FT-IR spectrum of the reaction between $1\text{-}^{15}\text{N}$ and 3 equiv. ArO^\bullet recorded in CH_2Cl_2 . Background solvent signals have been subtracted.	S35
Figure S31. Overlay of the FT-IR spectra of the reactions between 1 or $1\text{-}^{15}\text{N}$ with 3.0 equiv. ArO^\bullet in CH_2Cl_2 after workup. Background solvent signals have been subtracted.	S36
Figure S32. FT-IR spectrum of the reaction between 1 and 1.0 equiv. of ArO^\bullet recorded in CH_2Cl_2 after workup. Background solvent signals have been subtracted.	S36
Figure S33. Overlaid FT-IR spectra of the reactions between 1 and 1.0 equiv. (black) or 3.0 equiv. (red) ArO^\bullet recorded in CH_2Cl_2 after workup. Background solvent signals have been subtracted.	S37
Figure S34. $^{31}\text{P}\{^1\text{H}\}$ NMR spectrum of the reaction between 1 and 1, 2 and 3 sequentially added equivalents of ArO^\bullet in PhF.	S37
Figure S35. $^{31}\text{P}\{^1\text{H}\}$ NMR spectrum of 1 (bottom) or $1\text{-}^{15}\text{N}$ treated with 3 equiv. ArO^\bullet in PhF.	S38
Figure S36. $^{15}\text{N}\{^1\text{H}\}$ NMR spectrum of the reaction between $1\text{-}^{15}\text{N}$ and 3 ArO^\bullet in PhF. NT=20,000 scans.	S38
Figure S37. ^1H NMR spectrum of the pentane triturate of the reaction between 1 and 3.0 equiv. ArO^\bullet in toluene- D_8 corresponding to 2,4,6-tritertbutylphenol.	S39

Figure S38. FT-IR spectrum of the pentane triturate of the reaction between 1 and 3.0 equiv. ArO• corresponding to 2,4,6-tritertbutylphenol in <i>n</i> -hexane with background solvent signals subtracted.	S39
Figure S39. ³¹ P{ ¹ H} NMR spectrum of the reaction between 2 and 3 equiv. ArO• after 72 h in PhF at room temperature.	S40
Figure S40. ¹⁵ N NMR spectrum of the reaction between 2- ¹⁵ N and 3 equiv. ArO• in PhF at 298 K.	S40
Figure S41. ³¹ P{ ¹ H} NMR spectrum of the reaction between 2- ¹⁵ N and 3 equiv. ArO• in PhF at 298 K.	S41
Figure S42. ³¹ P{ ¹ H} NMR spectrum of the reaction between free dppe, 4 equiv. ArO• and NH ₃ in PhF after 16 h at 298K.	S41
Figure S43. ³¹ P{ ¹ H} NMR spectrum of the reaction between free dppe, 4 equiv. ArO• and NH ₃ in PhF after 16 h at 298K.	S42
Figure S44. Time-dependence of the reaction between 2- ¹⁵ N and 3 equiv. ArO• at 298 K in PhF. Starting Mn concentration: 38.3 mM.	S42
Figure S45. Superimposed time-dependence of the reaction between 2- ¹⁵ N and 3 equiv. ArO• at 298 K in PhF.	S43
Figure S46. Time-dependence of the reaction between 2- ¹⁵ N and 3 equiv. ArO• at 298 K in PhF. [Mn] ₀ = 19.6 mM.	S43
Figure S47. Superimposed time-dependence of the reaction between 2- ¹⁵ N and 3 equiv. ArO• at 298 K in PhF.	S44
Figure S48. Time-dependence of the reaction between 2- ¹⁵ N and 3 equiv. ArO• at 298 K in PhF. Starting Mn concentration: 19.6 mM.	S44
Figure S49. ³¹ P{ ¹ H} NMR spectra of the reaction between 2 (top) or 2- ¹⁵ N (bottom) with 3 equiv. ArO• in PhF.	S45
Figure S50. FT-IR spectrum of the reaction between 2 and 3.0 equiv. ArO• in CH ₂ Cl ₂ after workup. Background solvent signals have been subtracted.	S45
Figure S51. Comparison of IR spectra in the CO-stretching region for the overall conversion of Mn(dppe) ₂ (CO)Br to 2 + 3 equiv. ArO•.	S46
Figure S52. In situ IR spectra of the reaction between 2 and 4 equiv. ArO• in PhF to 8 h at 298 K, with emphasis on the Mn-CO region of the spectrum.	S46
Figure S53. In situ IR spectra of the reaction between 2 and 4 equiv. ArO• in PhF out to 24 min at 298 K, with emphasis on the Mn-CO region of the spectrum.	S47
Figure S54. In situ IR spectra of the reaction between 2 and 4 equiv. ArO• in PhF upon mixing at 298 K, with emphasis on the Mn-CO region of the spectrum.	S47
Figure S55. In situ IR spectrum of the reaction between 2 and 4 equiv. ArO• recorded in PhF at 5 min after mixing.	S48
Figure S56. In situ IR spectra of the reaction between 2 and 4 equiv. ArO•, showing spectra evolution between 48 (red) and 460 min (blue) recorded in PhF.	S48
Figure S57. In situ IR spectra of the reaction between 2 and 4 equiv. ArO• in PhF, comparing 2 with product spectrum after 27 min at 298 K.	S49

Figure S58. Cyclic voltammetry of 1 at 50 mV/s with and without exogenous base. Arrows indicate sweep origin and current scale. 0.1 M [Bu ₄ N]B(C ₆ F ₅) ₄ in PhF.....	S49
Figure S59. Cyclic voltammetry of 2 at 100 mV/s. Arrows indicate sweep origin and current scale. 0.2 M [Bu ₄ N]B(C ₆ F ₅) ₄ in PhF.....	S50
Figure S60. Cyclic voltammetry of 2 (2.0 mM) at 100 mV/s with 5 equiv. DBU added into the cell. Arrows show sweep origin and current scale. 0.2 M [Bu ₄ N]B(C ₆ F ₅) ₄ in PhF.	S50
Figure S61. Overlaid cyclic voltammograms of 2 (2.0 mM) at 100 mV/s and with 5 equiv. DBU added into the cell. Arrows show sweep origin and current scale. 0.2 M [Bu ₄ N]B(C ₆ F ₅) ₄ in PhF.	S51
Figure S62. Cyclic voltammetry of 2 (2.0 mM) with 5 equiv. DBU at different scan rates (25-800 mV/s). Arrows indicate sweep origin and current scale. 0.2 M [Bu ₄ N]B(C ₆ F ₅) ₄ in PhF.....	S51
Figure S63. Cyclic voltammetry of 2 (2.0 mM) showing the scan rate dependence from 25-1600 mV/s. Arrows show sweep origin and current scale.....	S52
References	S53

Experimental

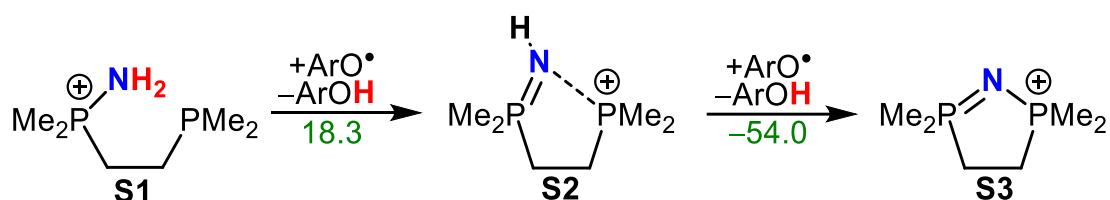
General Considerations

All reactions were carried out in a Vacuum Atmospheres Nexus glovebox under argon, or with standard Schlenk techniques. Atmospheric purity was determined by calibrated O₂ sensors and maintained at <0.3 ppm by purging for 5 min at 3 h intervals during use. Glassware was heated to 130 °C for at least one hour, then cooled under dynamic vacuum for 12 hours before use. THF, PhMe, n-hexane, n-pentane, fluorobenzene and dichloromethane were dried using an Innovative Technologies solvent purification system and were stored over freshly-activated 4 Å molecular sieves for 24 h. Fluorobenzene used in cyclic voltammetry was additionally distilled to remove electroactive impurities prior to data collection. PhMe-d₈, C₆D₅Br, and CDCl₃ were stirred over CaH₂ for ca. 12 h, then distilled and stored over freshly-activated molecular sieves. Mn(CO)₅Br (Sigma Aldrich), depe (Sigma Aldrich), dppe (Sigma Aldrich), KB(C₆F₅)₄ (Boulder Chemical), NaBAr^F₄ (SynQuest), and 2,4,6-tritertbutylphenol were acquired from commercial sources and used without further purification. Ammonia was acquired from Matheson (research purity, 99.9992%) and used as received by purging a Schlenk manifold for 5 minutes prior to use. ¹⁵NH₃ was acquired from Cambridge Isotope Laboratories (99.5% ¹⁵N) and used as received. 2,4,6-tritertbutylphenoxy radical, Mn(dppe)₂(CO)Br, [Mn(dppe)₂(CO)]BAr^F₄, Mn(depe)₂(CO)Br, [Mn(depe)₂(CO)]BAr^F₄, Mn(dppp)(dppm)(CO)Br, [Mn(dppp)(dppm)(CO)]BAr^F₄, and [Bu₄N]B(C₆F₅)₄ were prepared according to, or slightly modified, literature procedures.¹ Purity of Mn complexes were assayed and confirmed by ³¹P{¹H} NMR and FT-IR spectroscopy after each synthetic step.

¹H{¹³C}, ³¹P{¹H}, ¹³C{¹H}, ¹⁹F, and ¹⁵N{¹H} NMR were collected on an Agilent 500 MHz spectrometer and referenced to internal residual protio solvent signals (¹H, ¹³C), 85% H₃PO₄ at 0 ppm (³¹P), CF₃COOH at -77.5 ppm (¹⁹F), or CH₃NO₂ at 0 ppm (¹⁵N). NMR data were processed and figures prepared for publication using MestreNova Version 10.0.0. FT-IR were collected on a ThermoScientific Nicolet iS10 FT-IR spectrometer. Background solvent signals were subtracted via OMNIC software spectral math in absorbance mode using independently collected solvent-only scans, then converted to %transmittance. FT-IR spectra were prepared for publication using Origin 2017. ORTEP plots were generated from final .cif files in Mercury 3.10 and rendered as images using POVray. Cyclic Voltammetry (CV) was collected on a CH Instruments potentiostat in Cyclic Voltammetry mode. All CVs were collected with a three-electrode set up consisting of a 3 mm-diameter Glassy Carbon working electrode, a 1 mm-diameter glassy carbon counter electrode, and a Ag-wire pseudo reference electrode. All CVs were internally referenced to CoCp₂⁺⁰ at -1.33 V vs. Fe^{0/+} with 2.0 mM [CoCp₂]B(C₆F₅)₄. CVs of **2** were collected in distilled PhF with 2.0 mM analyte concentration and 0.2 M [Bu₄N]B(C₆F₅)₄. In situ infrared spectroscopy experiments were conducted on a Mettler-Toledo ReactIR 15 with an MCT detector, 7630.7 cm⁻¹ laser frequency and SiComp (silicon) probe connected via a 6 mm × 1.5 m AgX (silver halide) fiber. Spectra are averaged over 512 scans collected over 3 min intervals at 4 cm⁻¹ resolution. Background solvent (PhF) is subtracted from the resultant spectra and a first-order baseline correction applied.

Computational Details

Geometries were calculated using the B3LYP functional with the 6-31G** basis set on C, O, N, and P². Mn metal centers were calculated with the SDD basis set and effective core potential³. Frequency calculations at the same level were used to calculate zero-point energy. Entropic and enthalpic effects were obtained using a modified harmonic oscillator approximation which treats low-lying vibrational frequencies as free rotors.⁴ All energies were corrected for dispersion effects using the Grimme D3 correction with Becke-Johnson damping.⁵ The lack of imaginary frequencies was used to validate stationary points on the potential energy surface. Single point solvation energies in fluorobenzene were calculated using the SMD model of solvation.⁶ All calculations were carried out in ORCA 4.0⁷ These methods have been used previously to calculate thermodynamics for NH₃ oxidation reactions⁸ Coordinates for calculated geometries can be found in the accompanying XYZ coordinate file. They can be opened with a graphical viewing program such as Mercury (<https://www.ccdc.cam.ac.uk/mercury/>), which can be found online free of charge.



Scheme S1. Pathway for free dihydrophosphazanium reacting with ArO• radical. All free energies in kcal/mol.

To validate that the mechanism proposed involved metal coordination, we calculated the hydrogen atom transfer (HAT) reaction between free dihydrophosphazanium cation and ArO•, as shown in Scheme S1. At 18.3 kcal/mol, the first HAT is at least 4 kcal/mol higher in energy than for the metal-bound complexes. This high energy, combined with the inability of phosphazanium to form a stable L-type donor, lead us to believe that all of the observed chemistry occurs through the metal-coordinated complex.

Mn can adopt a wide variety of spin states, so these were calculated to ensure to the best of our ability that we were using the lowest energy complex. The absolute and relative free energies of complexes with different spins are show in Table S1.

Table S1. Spin State and Relative Energies for Computationally Determined Species.

Molecule	Absolute Free Energy [kcal/mol]	Spin state (S)	Relative Free Energy [kcal/mol]
A	-1326566.0	0	0.0
A	-1326542.0	1	24.0
A	-1326539.3	2	26.8
B	-1326169.0	1/2	0.0
B	-1326163.1	3/2	5.9
B	-1326167.1	5/2	1.9

C	-1325762.8	0	6.7
C	-1325769.5	1	0.0
C	-1325757.4	2	12.1
C	-1325747.7	3	21.8
D	-1325382.6	1/2	0.0
D	-1325369.8	3/2	12.7
D	-1325350.4	5/2	32.2
E	-1326160.2	1/2	0.0
E	-1326152.2	3/2	8.0
E	-1326153.0	5/2	7.2
F	-1325799.1	0	0.0
F	-1325798.4	1	0.7
F	-1325792.4	2	6.7
G	-1325425.1	1/2	0.0
G	-1325417.1	3/2	8.0
G	-1325416.6	5/2	8.5

Synthesis of New Complexes:

trans-[Mn(depe)₂(CO)(NH₃)]B(C₆F₅)₄ (**1**)

Under an argon atmosphere, a 20 mL scintillation vial was charged with a PTFE stir bar and 228 mg (0.194 mmol) [Mn(depe)₂(CO)]B(C₆F₅)₄, then dissolved in 15 mL PhF. The resulting dark blue solution was transferred to a 50 mL Schlenk flask fitted with ground glass joints and transferred to a Schlenk line fitted with N₂ and NH₃ purge lines. The Schlenk manifold was purged for 20 min with N₂, then with NH₃ for 5 min. The headspace of the flask was removed via 3 freeze-pump-thaw cycles. The Schlenk flask was back-filled with NH₃ (1 atm) while vigorously stirring, which resulted in a color change from dark blue to slightly greenish-yellow. The reaction was stirred for 5 min at room temperature, then the reaction mixture was frozen, and the headspace removed by vacuum. The Schlenk flask was returned to an argon atmosphere, and the volatiles removed under reduced pressure. The resulting tacky yellow solid was triturated with pentane (2 × 10 mL), and the yellow powder was dried under vacuum. Yield: 200 mg (86%). Single crystals suitable for X-ray diffraction were grown by slow evaporation from a saturated PhF solution into n-dodecane. ¹H NMR (PhF, 500 MHz, 298 K): δ(ppm), 1.83 (m, 8H, CH₂-CH₃), 1.62 (m, 4H, P(C₂H₄)P), 1.42 (m, 14H), 1.09 (m, 12H, CH₂-CH₃), 1.01(m, 12H), 0.26(s, 3H, NH₃). ³¹P{¹H} NMR (PhF, 202 MHz, 298 K): δ(ppm), 76.3. FT-IR (CH₂Cl₂): ν(cm⁻¹) 3386(w, N-H), 2942(w), 2911(w), 2884(w), 1823(s, CO), 1644(m), 1594(s), 1495(s), 1465(vs), 1218(s), 1155(w), 1085(w), 978(m).

trans-[Mn(depe)₂(CO)(¹⁵NH₃)]B(C₆F₅)₄ (**1-¹⁵N**)

Under an argon atmosphere, a 20 mL scintillation vial was charged with 65.0 mg (0.0554 mmol) [Mn(depe)₂(CO)]B(C₆F₅)₄ and dissolved in 1.2 mL PhF. This dark blue solution was transferred to two low pressure J. Young tubes and attached to a Schlenk manifold. Headspace was removed from each by two freeze-pump-thaw cycles. The gas-evacuated tubes were then transferred to a separate Swagelok manifold fitted with an ¹⁵NH₃ lecture cylinder (Cambridge Isotopes). The ammonia manifold was evacuated via three evacuate-refill cycles and the J. Young tube was back-filled with

$^{15}\text{NH}_3$. Shaking the tube resulted in an immediate color change from dark blue to bright yellow. After 60 seconds at room temperature, the solution was frozen, and the headspace removed by vacuum. *Note that this last step is critical for obtaining a good yield of this complex, as continued exposure to excess NH_3 results in decomposition.* Conversion to $\mathbf{1}$ - ^{15}N was confirmed by ^{31}P NMR spectroscopy, then brought back into an argon atmosphere. The contents of each tube were combined into the same 20 mL scintillation vial and each tube rinsed with fresh PhF. Volatiles were removed under reduced pressure to yield a yellow solid. The yellow solid was triturated with 2×5 mL n-pentane and dried *in vacuo* to yield a yellow powder. Yield: 80%. ^1H NMR (PhF, 500 MHz, 298 K): $\delta(\text{ppm})$, 1.79(m, 8H), 1.57(m, 4H, P-(C_2H_4)-P), 1.39(m, 14H), 1.04(m, 12H, - CH_2CH_3), 0.97(m, 12H, - CH_2CH_3), 0.21(d, $^1J_{\text{NH}}=65$ Hz, $^{15}\text{NH}_3$). $^{31}\text{P}\{^1\text{H}\}$ NMR (PhF, 202 MHz, 298 K): $\delta(\text{ppm})$, 76.4 (br, s, 4P). $^{15}\text{N}\{^1\text{H}\}$ NMR (PhF, 50.7 MHz, 298K): $\delta(\text{ppm})$, -416 (s).

[Mn(dppe) $_2$ (CO)(NH $_3$)]BAr $^{\text{F}_4}$, (2**)**

Under an argon atmosphere, a 20 mL scintillation vial was charged with a PTFE stir bar and 386 mg (0.221 mmol) [Mn(dppe) $_2$ (CO)]BAr $^{\text{F}_4}$, then dissolved 15 mL PhF. The resulting dark turquoise solution was transferred to a 50 mL Schlenk flask fitted with ground glass joints and transferred to a Schlenk line fitted with N_2 and NH_3 purge lines. The Schlenk manifold was purged for 20 min with N_2 , then with NH_3 for 5 min. The headspace of the flask was removed by 3 freeze-pump-thaw cycles. The Schlenk flask was back-filled with NH_3 while vigorously stirring, which resulted in a color change from dark blue to slightly greenish-yellow. The reaction was stirred for 5 min at room temperature, then returned to an argon atmosphere and the volatiles removed under reduced pressure. The resulting tacky orange-yellow solid was triturated 2×10 mL with pentane, and the orange-yellow powder was dried under vacuum. Yield: 386 mg (87%). Single crystals suitable for X-ray diffraction were grown by slow diffusion of n-pentane vapors into a saturated CH_2Cl_2 solution at room temperature. ^1H NMR (CDCl_3 , 500 MHz, 298 K): $\delta(\text{ppm})$, 7.73(s, BAr $^{\text{F}_4}$ Ar-o), 8H), 7.64(m, P-Ph, 8H), 7.51(s, BAr $^{\text{F}_4}$ Ar-p, 4H), 7.37(m, P-Ph, 8H), 7.21(m, P-Ph, 8H), 7.05(m, P-Ph, 8H), 6.42(m, P-Ph, 8H), 2.56(m, (P- C_2H_4 -P), 4H), 2.41(m, (P- C_2H_4 -P), 4H), 0.34(s, NH_3 , 3H). $^{13}\text{C}\{^1\text{H}\}$ NMR (CDCl_3 , 125 MHz, 298 K): $\delta(\text{ppm})$, 161.5(q, $^1J_{\text{CF}} = 56.2$ Hz), 136.0, 134.6, 132.5, 132.0, 131.3, 130.6, 130.3, 130.1, 129.3, 128.5, 128.7, 125.5, 123.3, 117.3, 30.1. $^{31}\text{P}\{^1\text{H}\}$ NMR (PhF, 202 MHz, 298 K): $\delta(\text{ppm})$, 82.8(br, 4P). ^{19}F (CDCl_3 , 470 MHz, 298 K): $\delta(\text{ppm})$, -62.4(s). FT-IR (CH_2Cl_2 , 298 K): $\nu(\text{cm}^{-1})$, 3346 (vw, N-H), 2961(w), 2931(w), 2873(w), 1826(m, C-O), 1646(w), 1514(s), 1464(vs), 1434(w), 1419(w), 1095(m).

[Mn(dppe) $_2$ (CO)($^{15}\text{NH}_3$)]BAr $^{\text{F}_4}$ (2**- ^{15}N)**

Under an argon atmosphere, a 20 mL scintillation vial was charged with 82.0 mg (0.0469 mmol) [Mn(dppe) $_2$ (CO)]BAr $^{\text{F}_4}$ and dissolved in 1.2 mL PhF. This dark blue solution was transferred to two low pressure J. Young tubes and attached to a Schlenk manifold. Headspace was removed from each via 2 freeze-pump-thaw cycles. The gas-evacuated tubes were then transferred to a separate Swagelok manifold fitting with $^{15}\text{NH}_3$. The ammonia manifold was evacuated via three evacuate-refill cycles and the J. Young tube back-filled with $^{15}\text{NH}_3$. *Note that generation of additional [Mn(dppe) $_2$ (CO) $_2$]BAr $^{\text{F}_4}$ impurity can be effectively prevented by this step.* Shaking the tube contents resulted in an immediate color change from dark blue to bright yellow. Conversion to $\mathbf{2}$ - ^{15}N was confirmed by ^{31}P NMR spectroscopy, then the tube was brought back into an argon atmosphere. The contents of each tube were combined into the same 20 mL scintillation vial and each tube rinsed with fresh PhF. Volatiles were removed under reduced pressure to yield a yellow

solid. The yellow solid was triturated with 2×5 mL n-pentane to yield a yellow powder. Yield: 80%. ^1H NMR (CDCl_3 , 500 MHz, 298 K): δ (ppm), 7.73(s, BAr^{F_4} Ar-o), 8H), 7.64(m, P-Ph, 8H), 7.51(s, BAr^{F_4} Ar-p, 4H), 7.37(m, P-Ph, 8H), 7.21(m, P-Ph, 8H), 7.05(m, P-Ph, 8H), 6.42(m, P-Ph, 8H), 2.56(m, (P- C_2H_4 -P), 4H), 2.41(m, (P- C_2H_4 -P), 4H), 0.30(dqt, $^1\text{J}_{\text{NH}} = 66$ Hz, $^3\text{J}_{\text{PH}} = 3.5$ Hz, $^{15}\text{NH}_3$, 3H). $^{31}\text{P}\{^1\text{H}\}$ NMR (PhF, 202 MHz, 298 K): δ (ppm), 82.9(br, 4P). $^{15}\text{N}\{^1\text{H}\}$ NMR (PhF, 50.7 MHz, 298 K): δ (ppm), -395.5 .

$[\text{Mn}(\text{dppp})(\text{dppm})(\text{CO})(^{15}\text{NH}_3)]\text{BAr}^{\text{F}_4}$ (5- ^{15}N**)**

Under an argon atmosphere, a 20 mL scintillation vial was charged with 33.5 mg (0.0192 mmol) $[\text{Mn}(\text{dppp})(\text{dppm})(\text{CO})]\text{BAr}^{\text{F}_4}$ and dissolved in 1.2 mL PhF. This dark blue solution was transferred to two low pressure J. Young tubes and attached to a Schlenk manifold. The headspace was removed by two freeze-pump-thaw cycles. The gas-evacuated tubes were then transferred to a separate Swagelok manifold fitted with $^{15}\text{NH}_3$. The ammonia manifold was evacuated via three evacuate-refill cycles and the J. Young tube back-filled with $^{15}\text{NH}_3$. Shaking the tube contents resulted in an immediate color change from dark blue to bright yellow. Conversion to **2- ^{15}N** was confirmed by ^{31}P NMR spectroscopy, then the tube was brought back into an argon atmosphere. The contents of each tube were combined into the same 20 mL scintillation vial and each tube rinsed with fresh PhF. Volatiles were removed under reduced pressure to yield a yellow solid. The yellow solid was triturated with 2×5 mL n-pentane to yield a yellow powder. Yield: 80%. $^{31}\text{P}\{^1\text{H}\}$ NMR (PhF, 202 MHz, 298 K): δ (ppm) 53.2(br, dppm, 2P), 25.1(br, dppp, 2P).

$[(\text{Et}_2\text{P}(\text{C}_2\text{H}_4)\text{PEt}_2)\text{N}]\text{B}(\text{C}_6\text{F}_5)_4$ and $[(\text{Et}_2\text{P}(\text{C}_2\text{H}_4)\text{PEt}_2)^{15}\text{N}]\text{B}(\text{C}_6\text{F}_5)_4$ (3 and 3- ^{15}N**)**

A 20 mL scintillation vial was charged with a PTFE stir bar, 12.9 mg (0.0492 mmol) ArO^\bullet and 1 mL PhF. This blue solution was cooled to -30°C . A separate vial was charged with 14.2 mg (0.0119 mmol) **1** or **1- ^{15}N** and 5 mL PhF, also cooled to -30°C . The cold PhF solution of **1** or **1- ^{15}N** was added dropwise to the stirring ArO^\bullet at a rate of 0.2 mL/min. The reaction was allowed to room to room temperature and stirred for 12 h. Volatiles were then removed under reduced pressure to yield an off-white solid. The solid was triturated with 3×5 mL n-pentane and the remaining powder dried in vacuo. Yield: 76% (^{31}P internal standard). Single crystals suitable for X-ray diffraction were grown via slow vapor diffusion of n-hexane vapors into a saturated PhF solution. The small amount of $[\text{Mn}(\text{depe})_2(\text{CO})_2]\text{B}(\text{C}_6\text{F}_5)_4$ side product prevented satisfactory elemental analysis. ^1H NMR (CDCl_3 500 MHz, 298 K): δ (ppm), 1.97(m, 3H), 1.85(m, 3H), 1.73(m, 4H), 1.20(m, 12H). $^{31}\text{P}\{^1\text{H}\}$ NMR (PhF, 262 MHz, 298 K) ^{14}N : 83.7 (s, 2P); ^{15}N : 83.7 (d, $^1\text{J}_{\text{PN}} = 40.5$ Hz, 2P). $^{15}\text{N}\{^1\text{H}\}$ (PhF, 50.7 MHz, 298 K): -341.2 ppm (t, $^1\text{J}_{\text{PN}} = 40.6$ Hz).

$[(\text{Ph}_2\text{P}(\text{C}_2\text{H}_4)\text{PPh}_2)\text{N}]\text{BAr}^{\text{F}_4}$ and $[(\text{Ph}_2\text{P}(\text{C}_2\text{H}_4)\text{PPh}_2)^{15}\text{N}]\text{BAr}^{\text{F}_4}$ (4 and 4- ^{15}N**)**

A 20 mL scintillation vial was charged with 28.1 mg (0.0161) **2** and 0.6 mL PhF. A separate vial was charged with 14.9 mg (0.0569 mmol) ArO^\bullet and the solution of **2** was added to this vial resulting in a color change to dark blue. The combined solution was transferred to a low-pressure J Young tube and the conversion to product was assayed at 24 h intervals by ^{31}P NMR until the product signal ceased growing in. Over this time, the color of the solution slowly became pale green, fading to goldenrod yellow after 72 h at 298 K. The J. Young tube was then brought back into an argon-filled glovebox and transferred to a 20 mL scintillation vial. The tube was rinsed with 2 mL PhF and volatiles removed under reduced pressure from the combined solution, resulting in an off-white solid. The solid was triturated with 3×5 mL n-pentane, and the triturate was assayed to confirm

ArOH generation. The remaining solid was dried under vacuum and isolated as an off-white powder. Yield: 29.6% (^{31}P internal standard). Single crystals suitable for X-ray diffraction were obtained via slow vapor diffusion of n-pentane vapors into a saturated CH_2Cl_2 solution. Crystals of the cyclophosphazene could be separated from this impurity; however both were found to crystallize together and independently under several crystal growth conditions. The $[\text{Mn}(\text{dppe})_2(\text{CO})_2]\text{BAr}^{\text{F}}_4$ side product in the isolated solid prevented satisfactory elemental analysis. $^{31}\text{P}\{^1\text{H}\}$ NMR (PhF, 202 MHz, 298 K): $\delta(\text{ppm})$, ^{14}N : 63.2 (s, 2P), ^{15}N : 63.2 (d, $^1J_{\text{PN}} = 38.4$ Hz, 2P). $^{15}\text{N}\{^1\text{H}\}$ NMR (PhF, 50.7 MHz, 298 K): $\delta(\text{ppm})$, -337 (t, $^1J_{\text{PN}} = 38.3$ Hz, 1N).

Crystallographic Details

[Mn(depe)₂(CO)(NH₃)]B(C₆F₅)₄ (1)

A pale yellow piece prepared from a feathery grown aggregate, measuring 0.17 × 0.10 × 0.08 mm³ was mounted on a loop with oil. Data was collected at -173°C on a Bruker APEX II single crystal X-ray diffractometer, Mo-radiation.

Crystal-to-detector distance was 40 mm and exposure time was 10 seconds per frame for all sets. The scan width was 0.5°. Data collection was 99.5% complete to 25° in θ . A total of 17542 merged reflections were collected covering the indices, $-9 \leq h \leq 9$, $-31 \leq k \leq 31$, $-28 \leq l \leq 28$. 8800 reflections were symmetry independent and the $R_{\text{int}} = 0.0741$ indicated that the data was of about average quality (0.07). Indexing and unit cell refinement indicated a primitive monoclinic lattice. The space group was found to be $P 2_1/c$ (No. 14).

The data was integrated and scaled using SAINT, SADABS within the APEX2 software package by Bruker.⁹

Solution by direct methods (SHELXT¹⁰ or SIR97¹¹) produced a complete heavy atom phasing model consistent with the proposed structure. The structure was completed by difference Fourier synthesis with SHELXL.¹² Scattering factors are from Waasmair and Kirfel.¹³ Hydrogen atoms were placed in geometrically idealised positions and constrained to ride on their parent atoms with C---H distances in the range 0.95-1.00 Angstrom. Isotropic thermal parameters U_{eq} were fixed such that they were 1.2 U_{eq} of their parent atom U_{eq} for CH's and 1.5 U_{eq} of their parent atom U_{eq} in case of methyl groups. All non-hydrogen atoms were refined anisotropically by full-matrix least-squares.

The crystals were not perfectly straight grown and exhibited striation marks and other signs of twinning. A merohedral twin law was discovered, implemented with twin matrix (-1 0 0, 0 1 0, 0 0 1), which partially obscured the extinctions related to the two-fold screw axis. Despite helpful application of the twin matrix, the overall R1 of the structure remained slightly elevated. One ethyl ligand (C19-C20) appeared disordered. The treatment of disorder required application of some restraints and about 0.5% of bad data was excluded.

Table S2: Crystallographic data for **1**.

Empirical formula	C ₄₅ H ₅₁ B F ₂₀ Mn N O P ₄
Formula weight	1191.49
Temperature	100(2) K
Wavelength	0.71073 Å
Crystal system	Monoclinic
Space group	P 2 ₁ /c
Unit cell dimensions	a = 8.0303(6) Å α = 90°. b = 26.226(2) Å β = 90.377(5)°. c = 23.4324(19) Å γ = 90°.
Volume	4934.8(7) Å ³
Z	4
Density (calculated)	1.604 Mg/m ³
Absorption coefficient	0.510 mm ⁻¹
F(000)	2424
Crystal size	0.170 x 0.100 x 0.080 mm ³
Theta range for data collection	1.553 to 25.188°.
Index ranges	-9 ≤ h ≤ 9, -31 ≤ k ≤ 31, -28 ≤ l ≤ 28
Reflections collected	17542
Independent reflections	8800 [R(int) = 0.0741]
Completeness to theta = 25.000°	99.5 %
Refinement method	Full-matrix least-squares on F ²
Data / restraints / parameters	8800 / 17 / 677
Goodness-of-fit on F ²	1.097
Final R indices [I > 2σ(I)]	R1 = 0.0898, wR2 = 0.1906
R indices (all data)	R1 = 0.1411, wR2 = 0.2093
Extinction coefficient	0.0166(9)
Largest diff. peak and hole	0.703 and -0.532 e.Å ⁻³

[Mn(dppe)₂(CO)(NH₃)]BAr^F₄ (2)

An orange block measuring 0.10 × 0.10 × 0.05 mm³ was mounted on a loop with oil. Data was collected at -173°C on a Bruker APEX II single crystal X-ray diffractometer, Mo-radiation.

Crystal-to-detector distance was 40 mm and exposure time was 10 seconds per frame for all sets. The scan width was 0.5°. Data collection was 99.5% complete to 25° in θ . A total of 153570 merged reflections were collected covering the indices, $-16 \leq h \leq 16$, $-23 \leq k \leq 23$, $-23 \leq l \leq 23$. 15989 reflections were symmetry independent and the $R_{\text{int}} = 0.0351$. Indexing and unit cell refinement indicated a primitive triclinic lattice. The space group was found to be P-1 (No. 2).

The data was integrated and scaled using SAINT, SADABS within the APEX2 software package by Bruker.⁹

Solution by direct methods (SHELXT¹⁰ or SIR97¹¹) produced a complete heavy atom phasing model consistent with the proposed structure. The structure was completed by difference Fourier synthesis with SHELXL.¹² Scattering factors are from Waasmair and Kirfel.¹³ Hydrogen atoms were placed in geometrically idealised positions and constrained to ride on their parent atoms with C---H distances in the range 0.95-1.00 Angstrom. Isotropic thermal parameters U_{eq} were fixed such that they were 1.2 U_{eq} of their parent atom U_{eq} for CH's and 1.5 U_{eq} of their parent atom U_{eq} in case of methyl groups. All non-hydrogen atoms were refined anisotropically by full-matrix least-squares.

Table S3. Crystallographic data for **2**

Empirical formula	C ₅₃ H ₅₁ MnNOP ₄ ·C ₃₂ H ₁₂ BF ₂₄ ·2(CH ₂ Cl ₂)	
Formula weight	1929.84	
Temperature	100(2) K	
Wavelength	0.71073 Å	
Crystal system	Triclinic	
Space group	P -1	
Unit cell dimensions	a = 13.128 (5) Å	α=96.069 (12)°.
	b = 18.154 (6) Å	β=92.463 (14)°.
	c = 18.203 (6) Å	γ=99.009 (15)°.
Volume	4253 (2) Å ³	
Z	2	
Density (calculated)	1.507 Mg/m ³	
Absorption coefficient	0.460 mm ⁻¹	
F(000)	1956	
Crystal size	0.100 x 0.100 x 0.050 mm ³	
Theta range for data collection	3.1 to 27.2°.	
Index ranges	-16≤h≤16, -23≤k≤23, -23≤l≤23	
Reflections collected	153570	
Independent reflections	15989 [R(int) = 0.035]	
Completeness to theta = 25.000°	99.6 %	
Refinement method	Full-matrix least-squares on F ²	
Data / restraints / parameters	18945 / 357 / 1206	
Goodness-of-fit on F ²	1.021	
Final R indices [I>2σ(I)]	R1 = 0.0537, wR2 = 0.1273	
R indices (all data)	R1 = 0.0656, wR2 = 0.1379	
Largest diff. peak and hole	1.53 and -0.92 e.Å ⁻³	

[(Et₂P(C₂H₄)PEt₂)N]B(C₆F₅)₄ (3)

A colorless plate, measuring 0.10 × 0.10 × 0.03 mm³ was mounted on a loop with oil. Data was collected at -173°C on a Bruker APEX II single crystal X-ray diffractometer, Mo-radiation.

Crystal-to-detector distance was 40 mm and exposure time was 30 seconds per frame for all sets. The scan width was 0.75°. Data collection was 100% complete to 25° in θ . A total of 17944 merged reflections were collected covering the indices, $-14 \leq h \leq 14$, $-16 \leq k \leq 16$, $-20 \leq l \leq 20$. 9042 reflections were symmetry independent and the $R_{\text{int}} = 0.0743$ indicated that the data was of average quality (0.07). Indexing and unit cell refinement indicated a triclinic lattice. The space group was found to be $P \bar{1}$ (No. 2).

The data was integrated and scaled using SAINT, SADABS within the APEX2 software package by Bruker.⁹

Solution by direct methods (SHELXT¹⁰ or SIR97¹¹) produced a complete heavy atom phasing model consistent with the proposed structure. The structure was completed by difference Fourier synthesis with SHELXL.¹² Scattering factors are from Waasmair and Kirfel.¹³ Hydrogen atoms were placed in geometrically idealised positions and constrained to ride on their parent atoms with C---H distances in the range 0.95-1.00 Angstrom. Isotropic thermal parameters U_{eq} were fixed such that they were 1.2 U_{eq} of their parent atom U_{eq} for CH's and 1.5 U_{eq} of their parent atom U_{eq} in case of methyl groups. All non-hydrogen atoms were refined anisotropically by full-matrix least-squares.

The structure contains about one half of disordered water per salt. As a result of presence/absence and disorder one ethyl group (C1-C2) in the vicinity shows 3:1 disorder as well.

Table S4: Crystallographic data for **3**.

Empirical formula	C ₃₄ H _{24.50} B F ₂₀ N O _{0.25} P ₂	
Formula weight	903.79	
Temperature	100(2) K	
Wavelength	0.71073 Å	
Crystal system	Triclinic	
Space group	P -1	
Unit cell dimensions	a = 10.9026(7) Å	α = 69.272(4)°.
	b = 12.5479(9) Å	β = 70.857(4)°.
	c = 15.0949(9) Å	γ = 78.274(4)°.
Volume	1815.7(2) Å ³	
Z	2	
Density (calculated)	1.653 Mg/m ³	
Absorption coefficient	0.252 mm ⁻¹	
F(000)	905	
Crystal size	0.100 x 0.100 x 0.030 mm ³	
Theta range for data collection	1.502 to 28.329°.	
Index ranges	-14 ≤ h ≤ 14, -16 ≤ k ≤ 16, -20 ≤ l ≤ 20	
Reflections collected	17944	
Independent reflections	9042 [R(int) = 0.0743]	
Completeness to theta = 25.000°	100.0 %	
Refinement method	Full-matrix least-squares on F ²	
Data / restraints / parameters	9042 / 3 / 538	
Goodness-of-fit on F ²	1.014	
Final R indices [I > 2σ(I)]	R1 = 0.0498, wR2 = 0.1035	
R indices (all data)	R1 = 0.1091, wR2 = 0.1264	
Largest diff. peak and hole	0.642 and -0.477 e.Å ⁻³	

[(Ph₂P(C₂H₄)PPh₂)N]BAr^F₄ (4)

A thin colorless plate with ellipsoidal shape, measuring $0.33 \times 0.12 \times 0.02 \text{ mm}^3$ was mounted on a loop with oil. Data was collected at -173°C on a Bruker APEX II single crystal X-ray diffractometer, Mo-radiation.

Crystal-to-detector distance was 40 mm and exposure time was 10 seconds per frame for all sets. The scan width was 0.5° . Data collection was 100% complete to 25° in θ . A total of 25662 reflections were collected covering the indices, $-24 \leq h \leq 24$, $-23 \leq k \leq 23$, $-21 \leq l \leq 21$. 6779 reflections were symmetry independent and the $R_{\text{int}} = 0.0882$ indicated that the data was of average quality. Indexing and unit cell refinement indicated a C-centered monoclinic lattice. The space group was found to be C 2/c (No. 15).

The data was integrated and scaled using SAINT, SADABS within the APEX2 software package by Bruker.⁹

Solution by direct methods (SHELXT¹⁰ or SIR97¹¹) produced a complete heavy atom phasing model consistent with the proposed structure. The structure was completed by difference Fourier synthesis with SHELXL.¹² Scattering factors are from Waasmair and Kirfel.¹³ Hydrogen atoms were placed in geometrically idealised positions and constrained to ride on their parent atoms with C---H distances in the range 0.95-1.00 Angstrom. Isotropic thermal parameters U_{eq} were fixed such that they were $1.2U_{\text{eq}}$ of their parent atom U_{eq} for CH's and $1.5U_{\text{eq}}$ of their parent atom U_{eq} in case of methyl groups. All non-hydrogen atoms were refined anisotropically by full-matrix least-squares.

Both salt molecules are completed by lattice symmetry.

Table S5: Crystallographic data for **4**.

Empirical formula	C58 H36 B F24 N P2
Formula weight	1275.63
Temperature	100(2) K
Wavelength	0.71073 Å
Crystal system	Monoclinic
Space group	C 2/c
Unit cell dimensions	a = 18.4668(16) Å $\alpha = 90^\circ$. b = 17.8732(16) Å $\beta = 95.476(6)^\circ$. c = 16.6797(14) Å $\gamma = 90^\circ$.
Volume	5480.2(8) Å ³
Z	4
Density (calculated)	1.546 Mg/m ³
Absorption coefficient	0.202 mm ⁻¹
F(000)	2568
Crystal size	0.330 x 0.120 x 0.020 mm ³
Theta range for data collection	1.589 to 28.360°.
Index ranges	-24 ≤ h ≤ 24, -23 ≤ k ≤ 23, -21 ≤ l ≤ 21
Reflections collected	25662
Independent reflections	6779 [R(int) = 0.0882]
Completeness to theta = 25.000°	100.0 %
Refinement method	Full-matrix least-squares on F ²
Data / restraints / parameters	6779 / 0 / 389
Goodness-of-fit on F ²	1.022
Final R indices [I > 2σ(I)]	R1 = 0.0543, wR2 = 0.1304
R indices (all data)	R1 = 0.1061, wR2 = 0.1568
Largest diff. peak and hole	0.530 and -0.572 e.Å ⁻³

[Mn(dppe)₂(CO)₂]BAr^F₄

A yellow plate, measuring 0.18 x 0.17 x 0.02 mm³ was mounted on a loop with oil. Data was collected at -173°C on a Bruker APEX II single crystal X-ray diffractometer, Mo-radiation.

Crystal-to-detector distance was 42 mm and exposure time was 10 seconds per frame for all sets. The scan width was 0.5°. Data collection was 98.8% complete to 25° in θ . A total of 14403 reflections were collected covering the indices, $-14 \leq h \leq 14$, $-22 \leq k \leq 22$, $-43 \leq l \leq 44$. 7645 reflections were symmetry independent and the $R_{\text{int}} = 0.0544$ indicated that the data was of good quality. Indexing and unit cell refinement indicated a primitive orthorhombic lattice. The space group was found to be $Pbcn$ (No. 57).

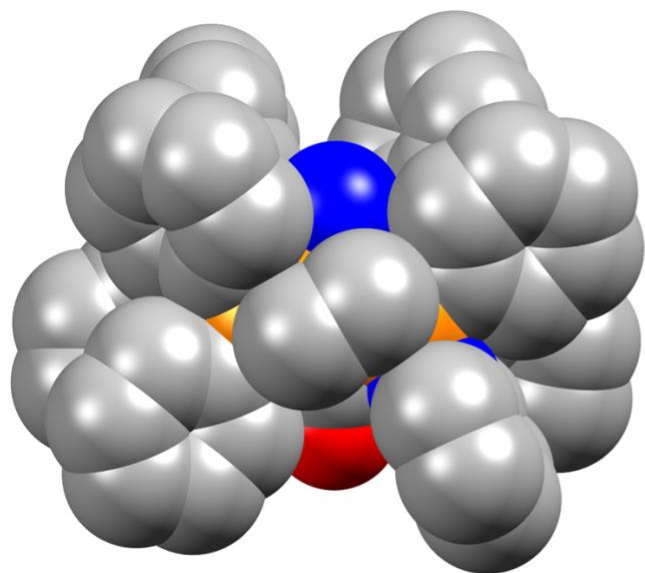
The data was integrated and scaled using SAINT, SADABS within the APEX2 software package by Bruker.⁹

The contribution of disordered solvent to the diffraction pattern was removed with SQUEEZE.¹⁵

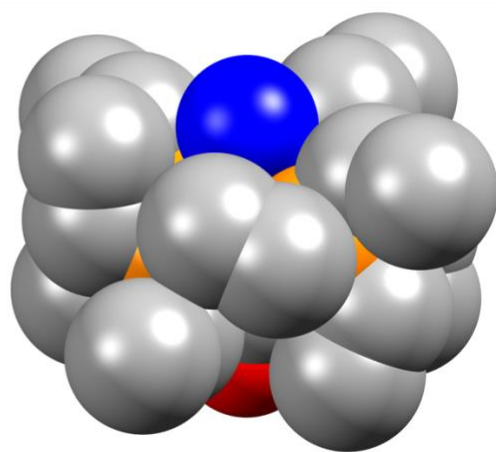
Solution by direct methods (SHELXT¹⁰ or SIR97¹¹) produced a complete heavy atom phasing model consistent with the proposed structure. The structure was completed by difference Fourier synthesis with SHELXL.¹² Scattering factors are from Waasmair and Kirfel.¹³ Hydrogen atoms were placed in geometrically idealised positions and constrained to ride on their parent atoms with C---H distances in the range 0.95-1.00 Angstrom. Isotropic thermal parameters U_{eq} were fixed such that they were $1.2U_{\text{eq}}$ of their parent atom U_{eq} for CH's and $1.5U_{\text{eq}}$ of their parent atom U_{eq} in case of methyl groups. All non-hydrogen atoms were refined anisotropically by full-matrix least-squares. Both half-salt-molecules are completed via symmetry.

Table S6: Crystallographic data for [Mn(dppe)₂(CO)₂]BAr^F₄.

Empirical formula	C ₈₆ H ₆₀ B F ₂₄ Mn O ₂ P ₄
Formula weight	1770.97
Temperature	100(2) K
Wavelength	0.71073 Å
Crystal system	Orthorhombic
Space group	P b c m
Unit cell dimensions	a = 12.1290(11) Å α = 90°. b = 18.6974(17) Å β = 90°. c = 36.581(3) Å γ = 90°.
Volume	8295.9(13) Å ³
Z	4
Density (calculated)	1.418 Mg/m ³
Absorption coefficient	0.337 mm ⁻¹
F(000)	3592
Crystal size	0.180 x 0.170 x 0.020 mm ³
Theta range for data collection	2.001 to 25.348°.
Index ranges	-14 ≤ h ≤ 14, -22 ≤ k ≤ 22, -43 ≤ l ≤ 44
Reflections collected	14403
Independent reflections	7645 [R(int) = 0.0544]
Completeness to theta = 25.000°	98.8 %
Refinement method	Full-matrix least-squares on F ²
Data / restraints / parameters	7645 / 0 / 540
Goodness-of-fit on F ²	1.028
Final R indices [I > 2σ(I)]	R1 = 0.0686, wR2 = 0.1601
R indices (all data)	R1 = 0.1076, wR2 = 0.1811
Largest diff. peak and hole	0.929 and -0.699 e.Å ⁻³



$[\text{Mn}(\text{dppe})_2(\text{CO})(\text{NH}_3)]^+$



$[\text{Mn}(\text{depe})_2(\text{CO})(\text{NH}_3)]^+$

Figure S1. Space-filling diagram comparing **2** (left) and **1** (right).

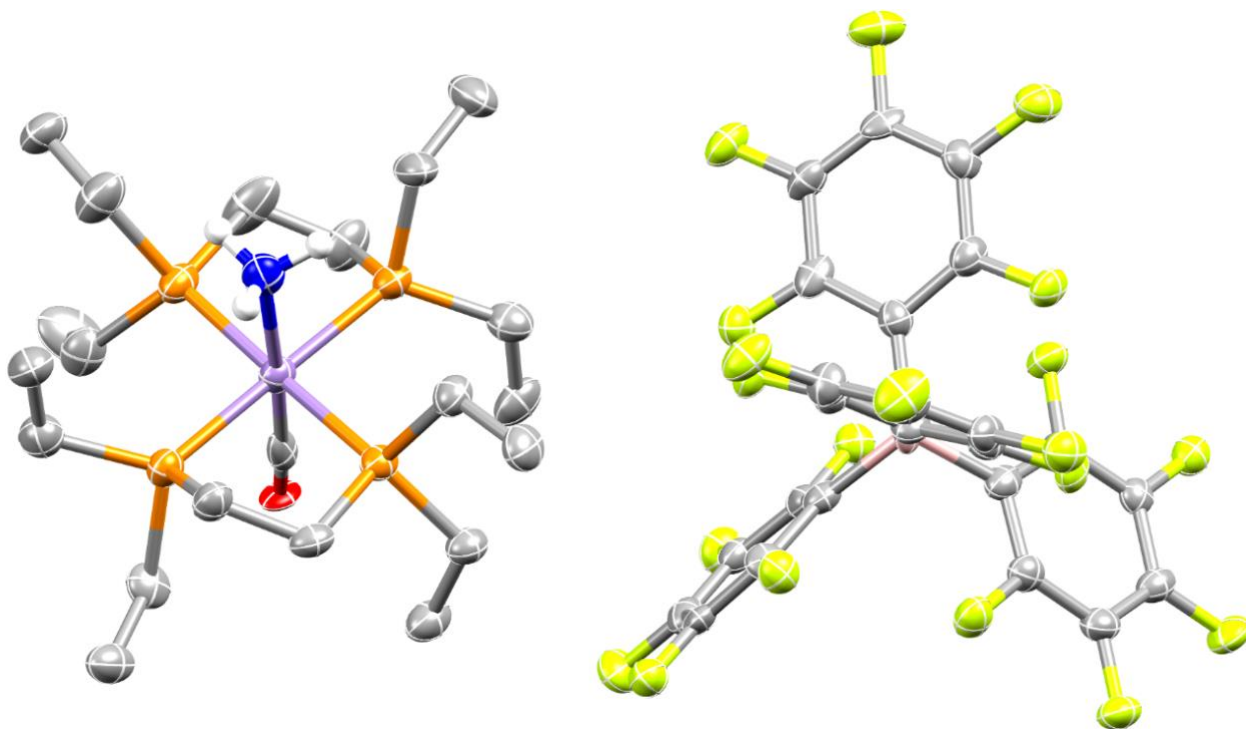


Figure S2. ORTEP representation of the cation-anion pair of **1**.

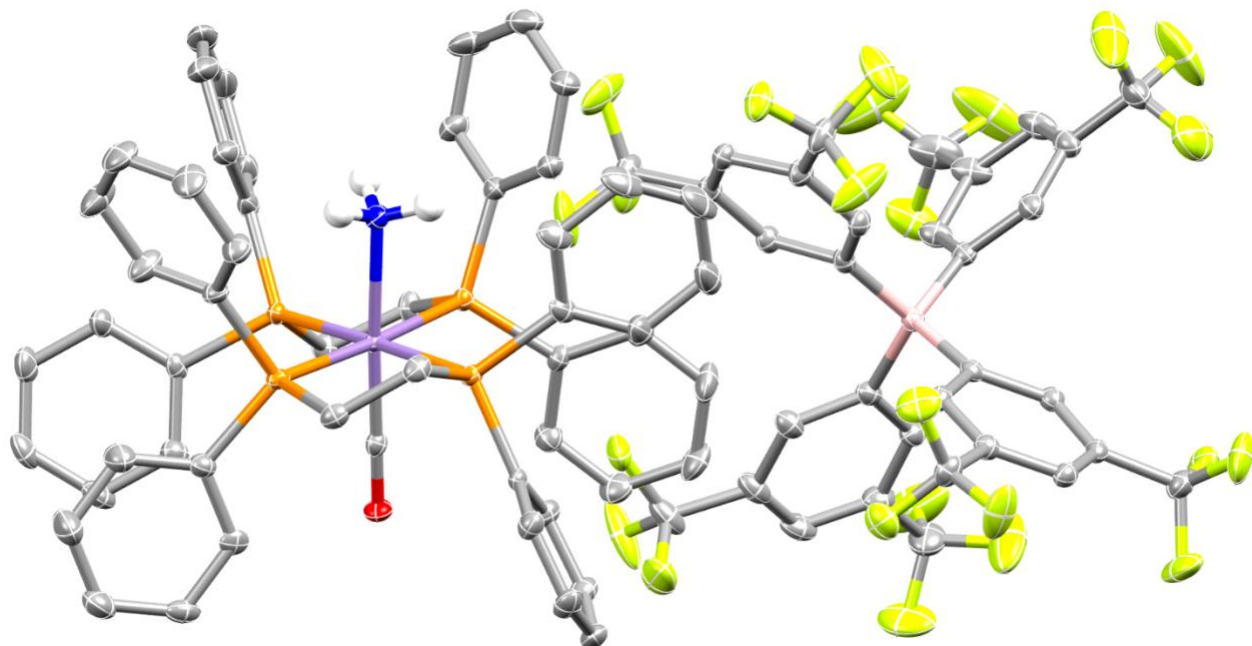


Figure S3. ORTEP representation of the cation-anion pair for **2**.

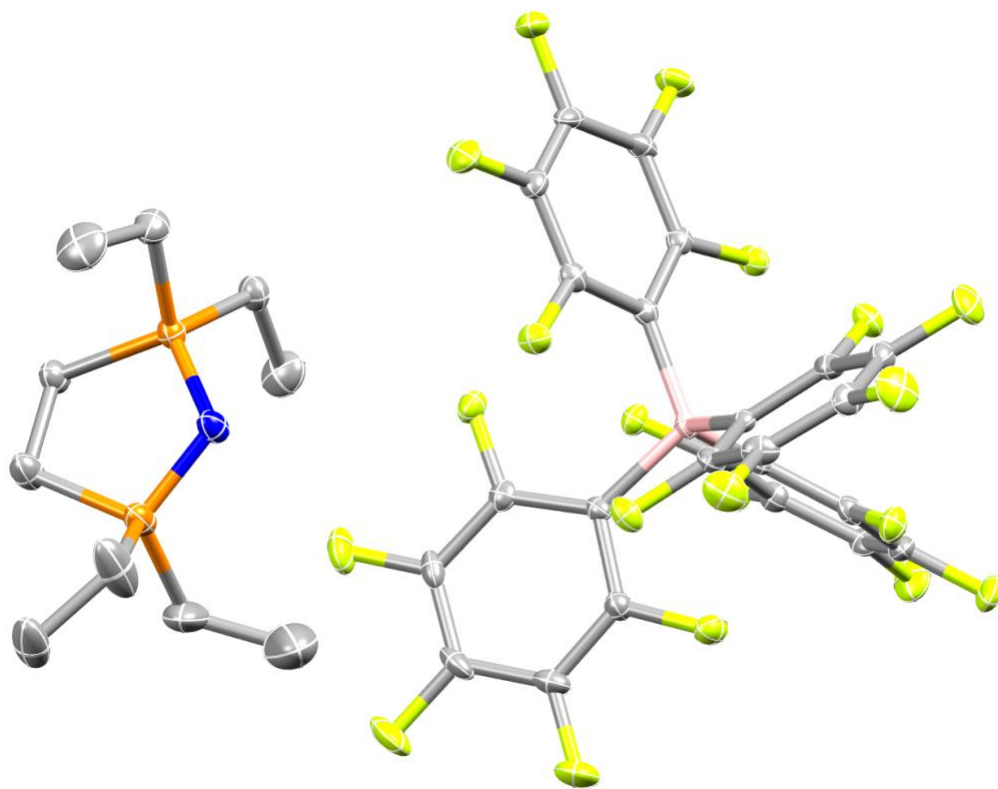


Figure S4. ORTEP representation of cation-anion pair of **3**. Hydrogen atoms and lattice guests have been removed for clarity.

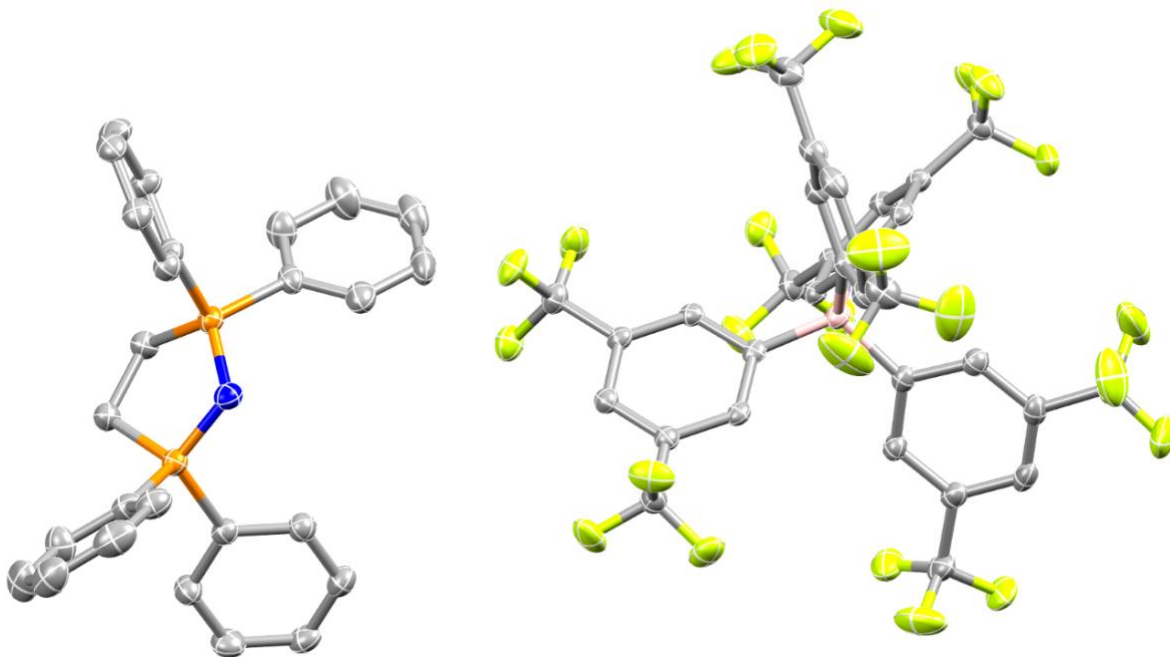


Figure S5. ORTEP representation (50% ellipsoid probability) of **4**. Hydrogen atoms have been removed for clarity.

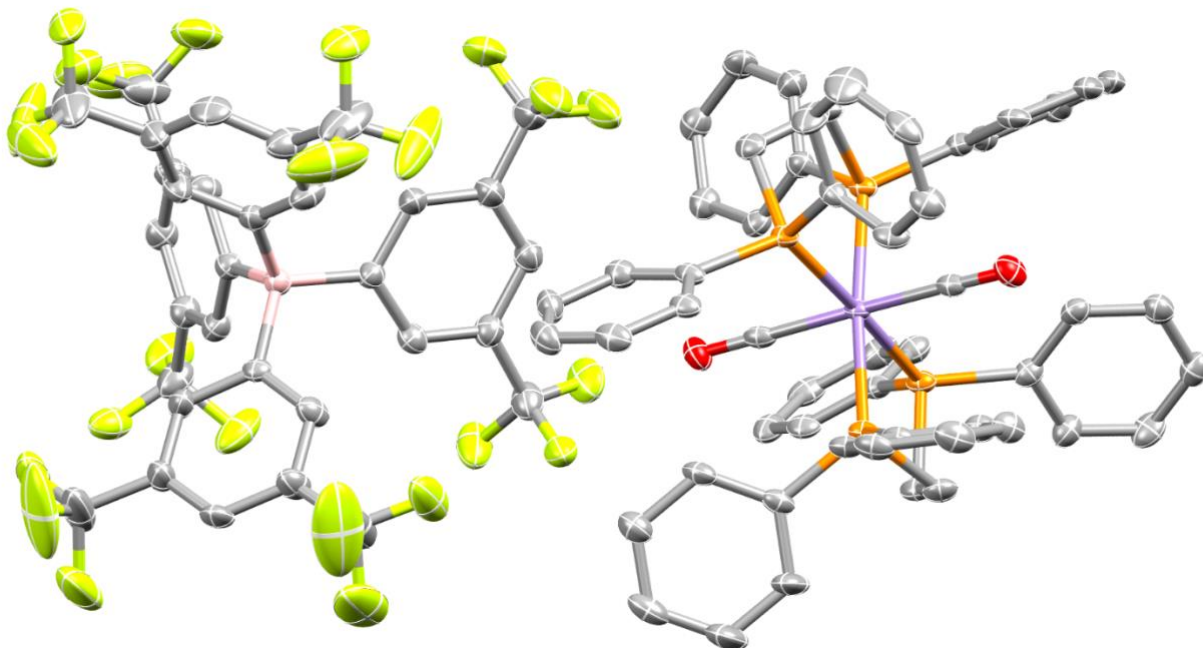


Figure S6. ORTEP representation of $[\text{Mn}(\text{dppe})_2(\text{CO})_2]\text{BARF}_4$, isolated from the same reaction mixture along with **4**.

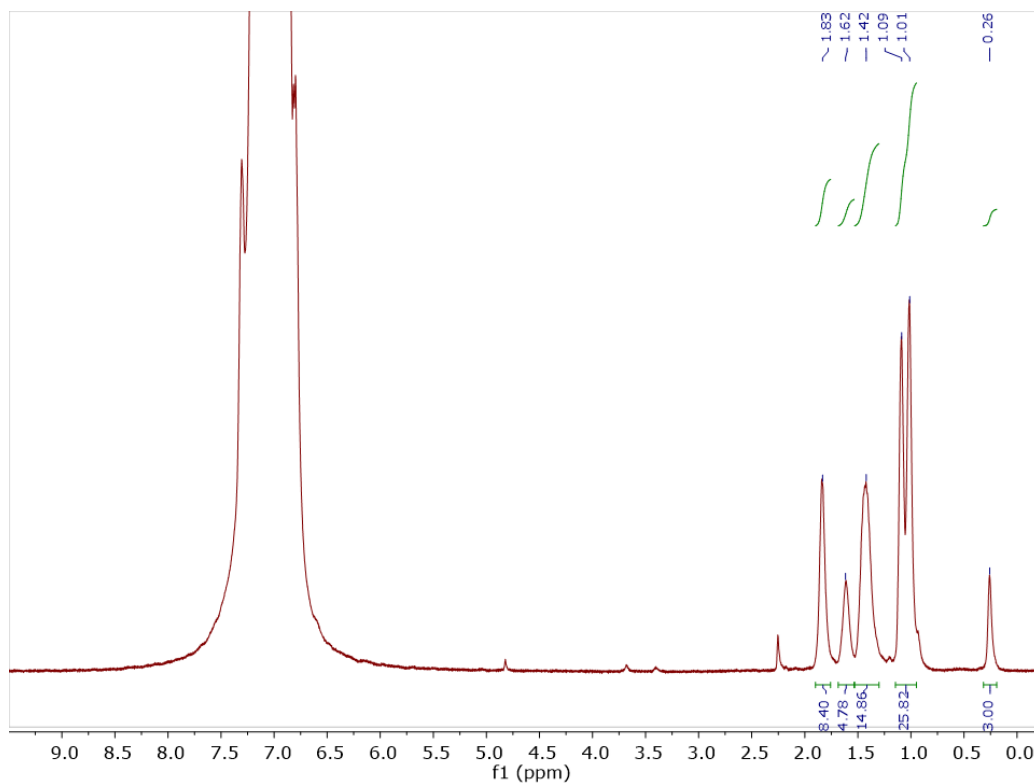


Figure S7. ^1H NMR spectrum of **1** in PhF.

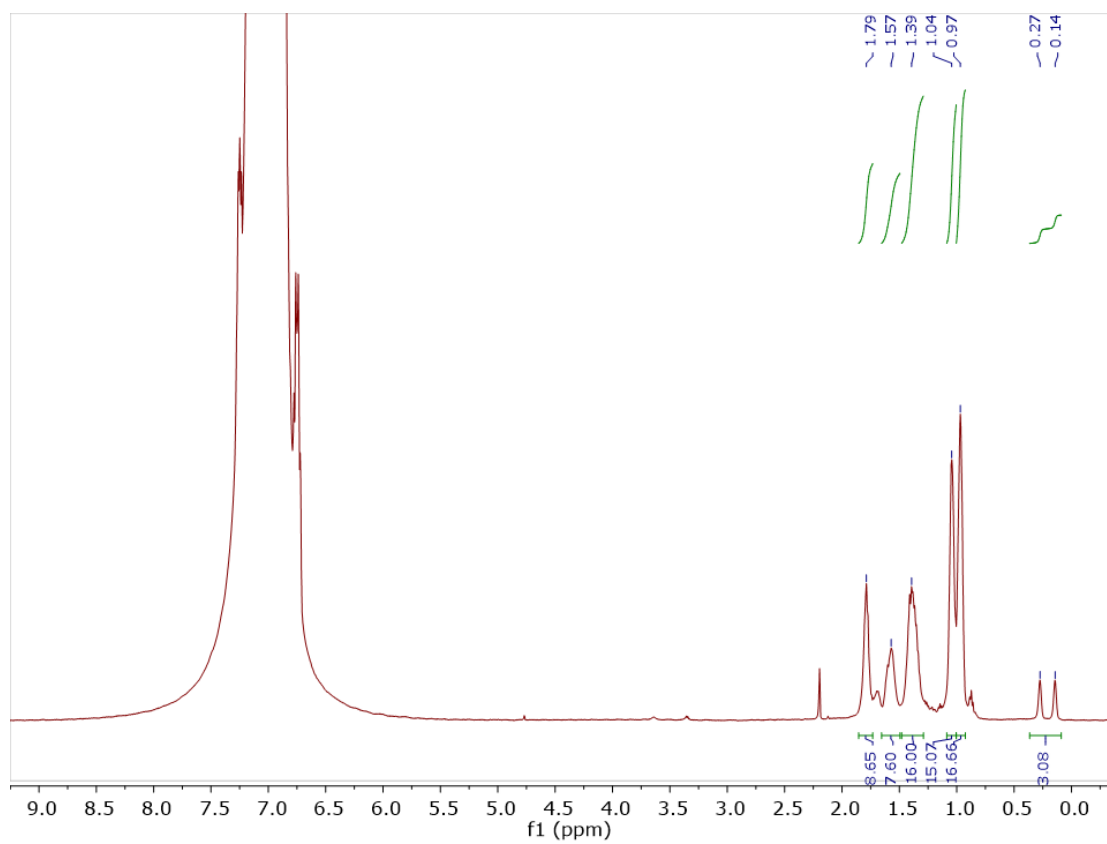


Figure S8. ^1H NMR spectrum of **1**- ^{15}N in PhF.

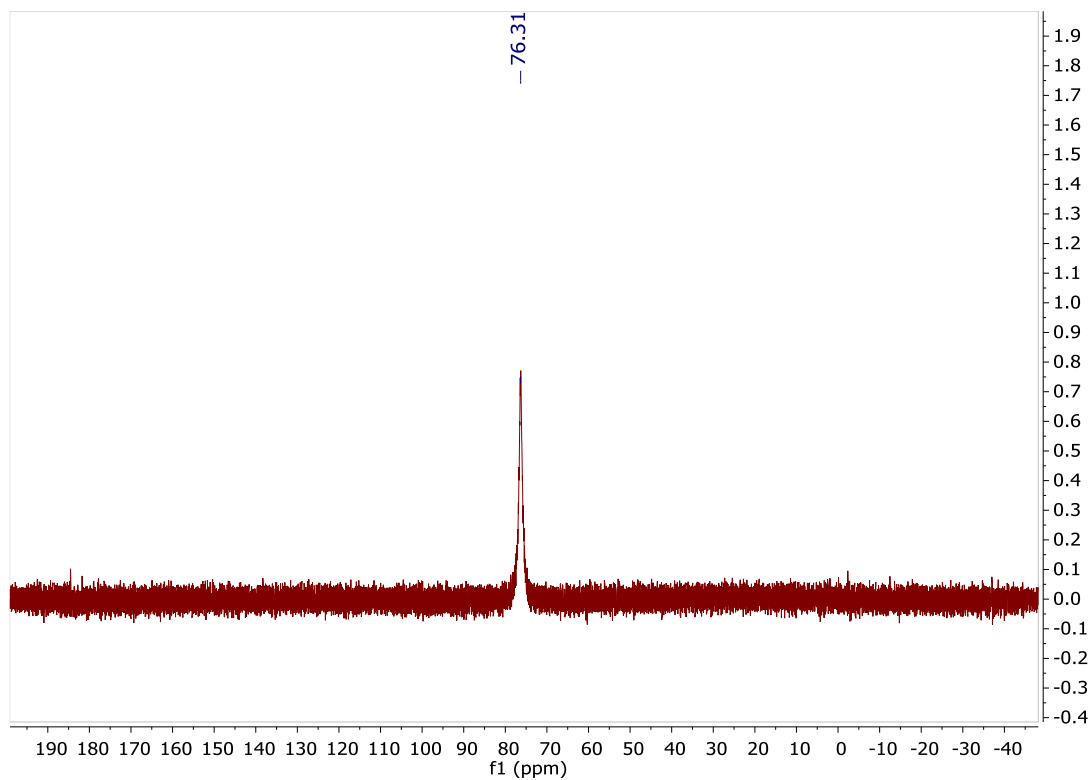


Figure S9. $^{31}\text{P}\{^1\text{H}\}$ NMR spectrum of **1** in PhF after crystallization and isolation.

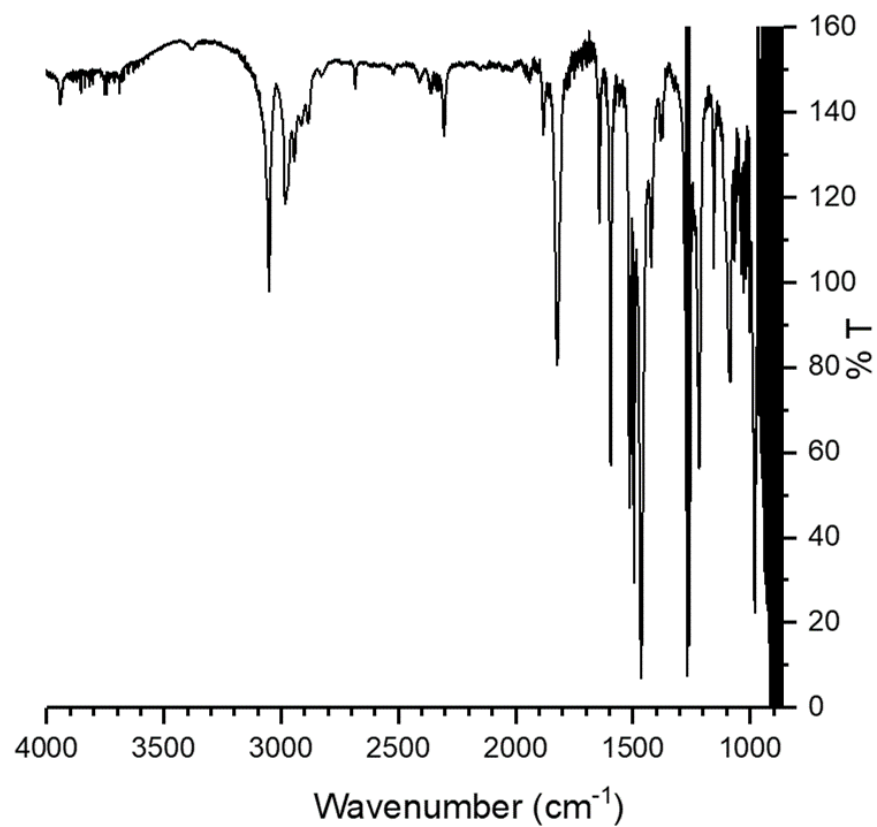


Figure S10. FT-IR spectrum of **1** in CH_2Cl_2 , with background signal subtracted.

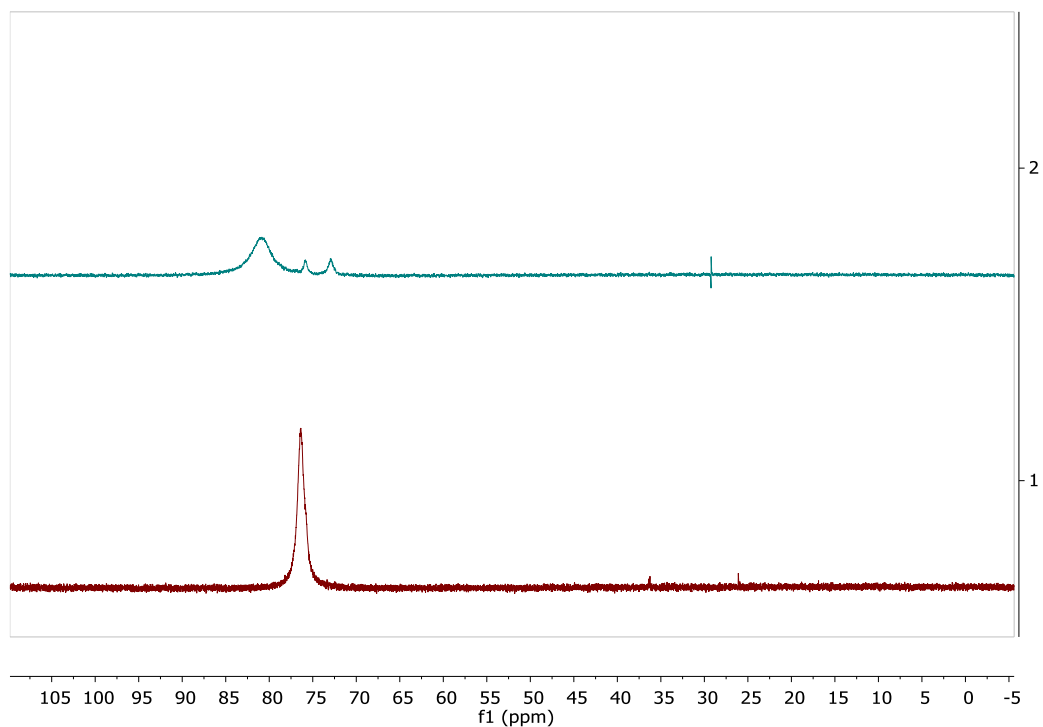


Figure S11. $^{31}\text{P}\{^1\text{H}\}$ NMR spectrum of $[\text{Mn}(\text{depe})_2(\text{CO})]\text{B}(\text{C}_6\text{F}_5)_4$ before (top) and after (bottom) addition of NH_3 in PhF.

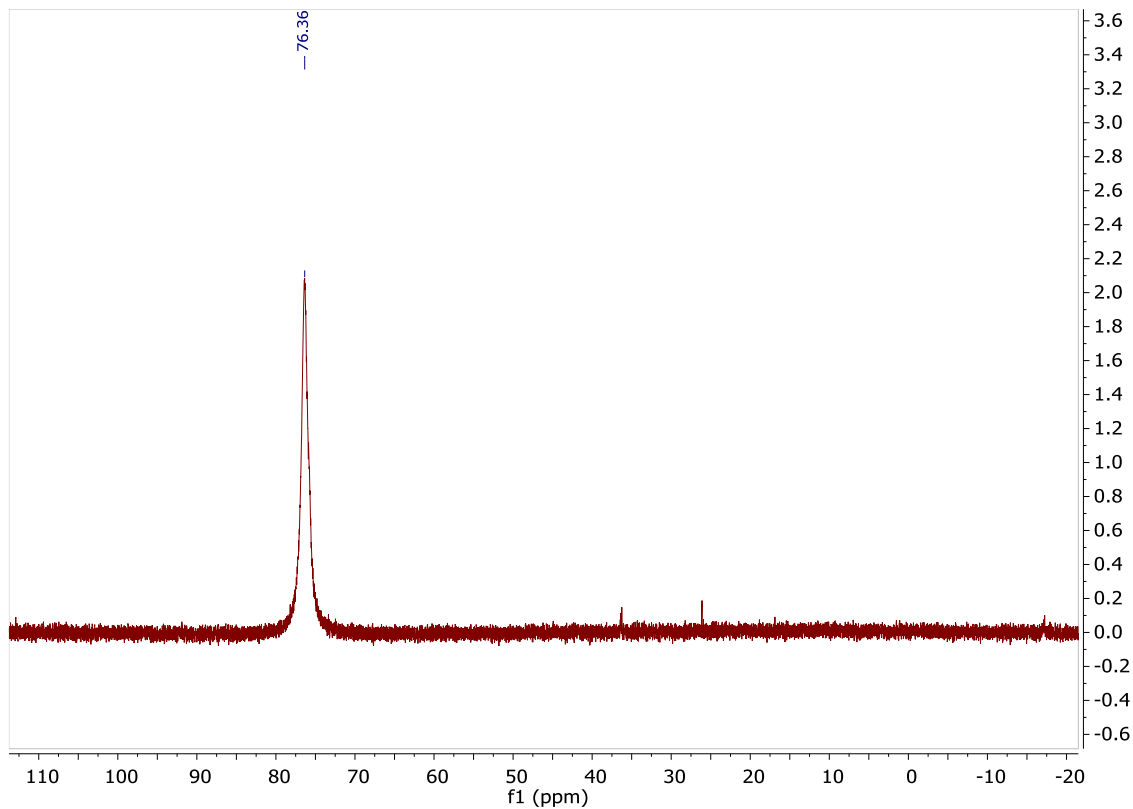


Figure S12. $^{31}\text{P}\{^1\text{H}\}$ NMR spectrum of as-synthesized $1\text{-}^{15}\text{N}$ in PhF.

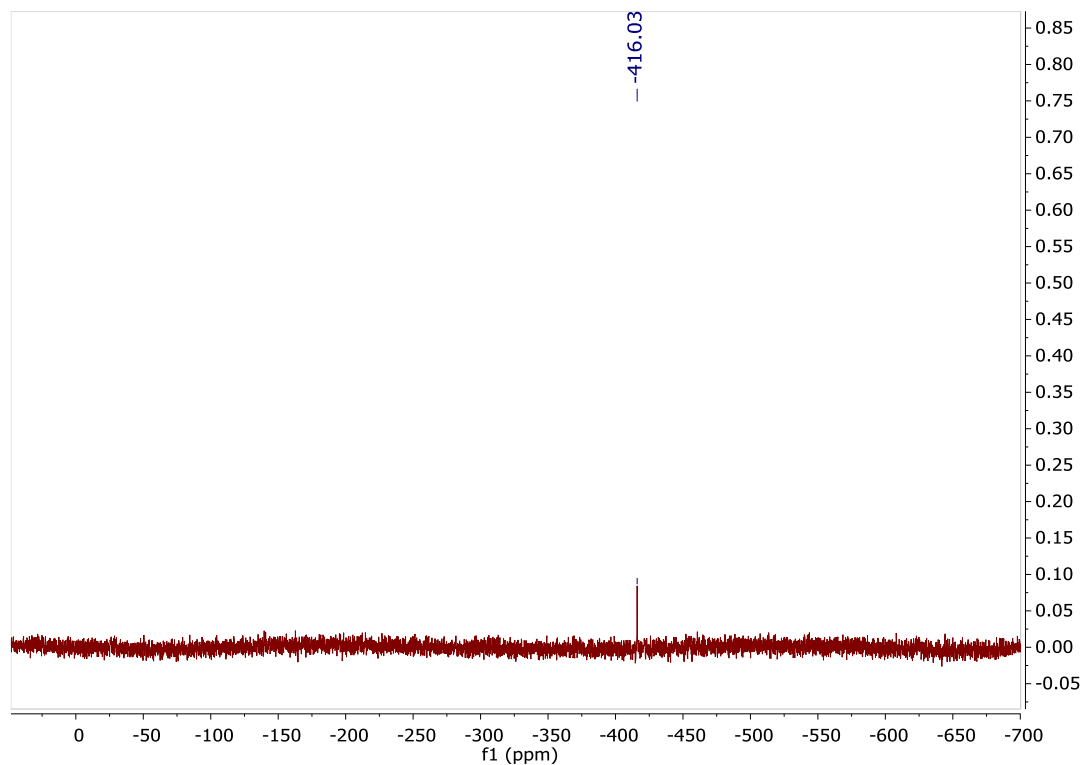


Figure S13. $^{15}\text{N}\{^1\text{H}\}$ NMR spectrum of $1\text{-}^{15}\text{N}$ in PhF.

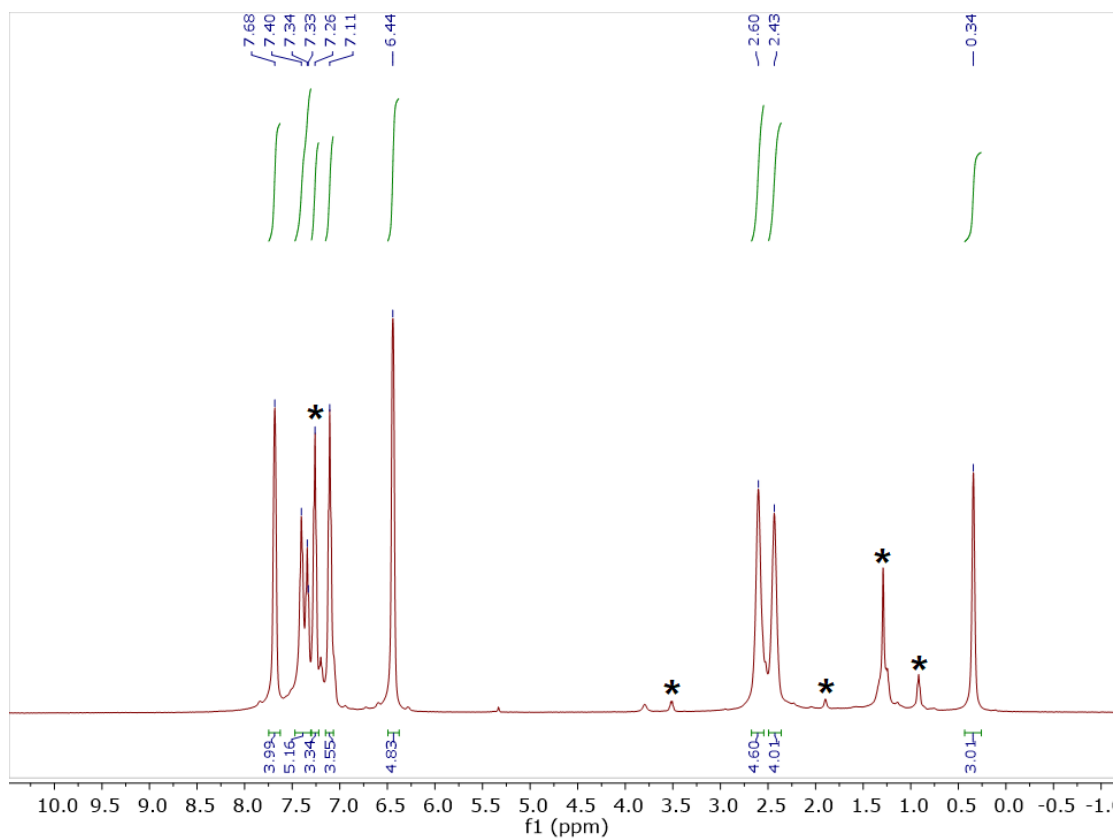


Figure S14. ^1H NMR spectrum of $2^+\text{B}(\text{C}_6\text{F}_5)_4^-$ in CDCl_3 . * denotes solvent-derived impurities.

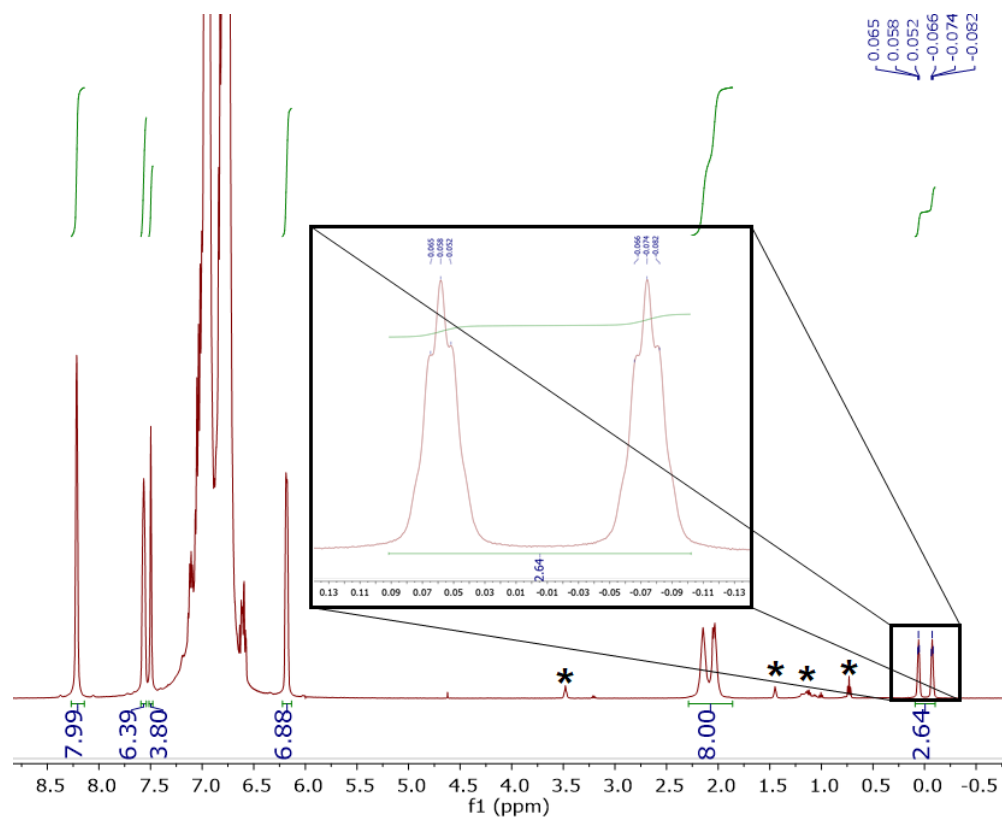


Figure S15. ^1H NMR spectrum recorded in PhF of $2\text{-}^{15}\text{N}$. Inset shows an expansion of the NH_3 signal and coupling. * denotes solvent-derived impurities.

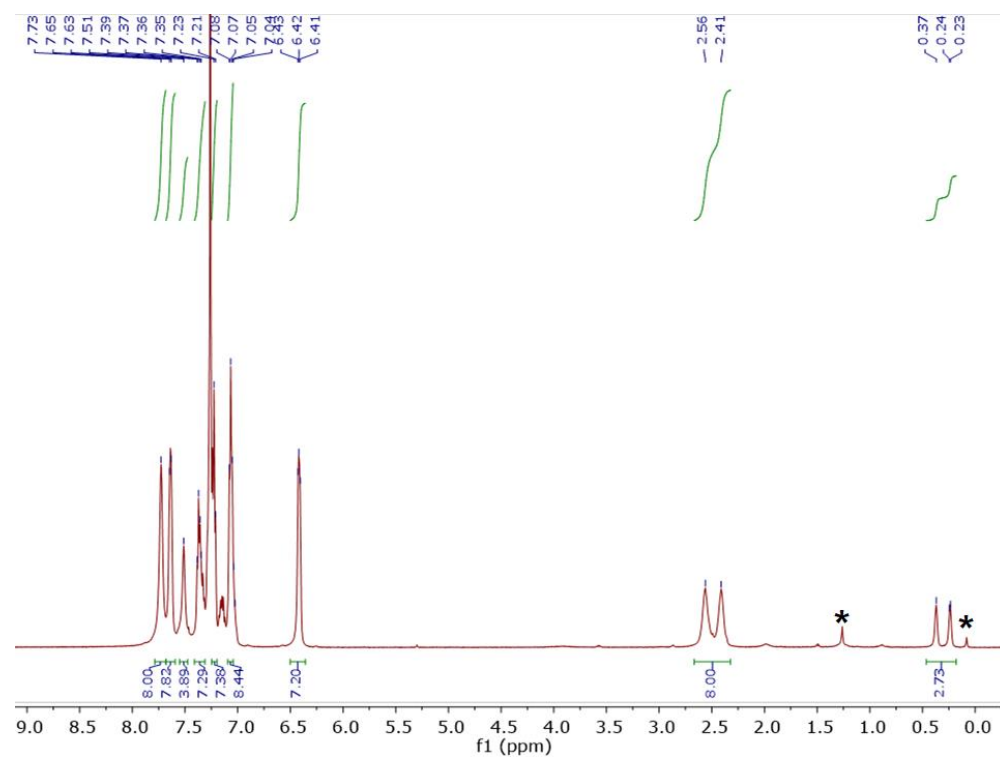


Figure S16. ^1H NMR spectrum of $2\text{-}^{15}\text{N}$ in CDCl_3 . * denotes solvent-derived impurities.

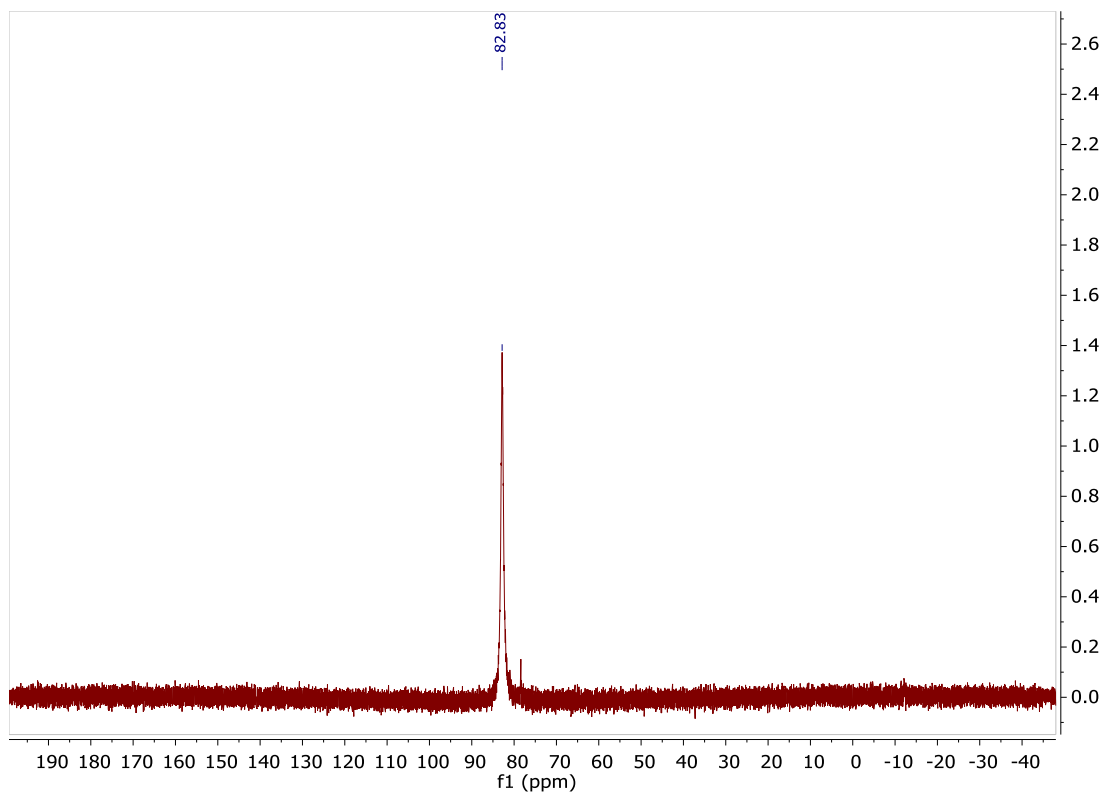


Figure S17. $^{31}\text{P}\{^1\text{H}\}$ NMR spectrum of **2** in PhF.

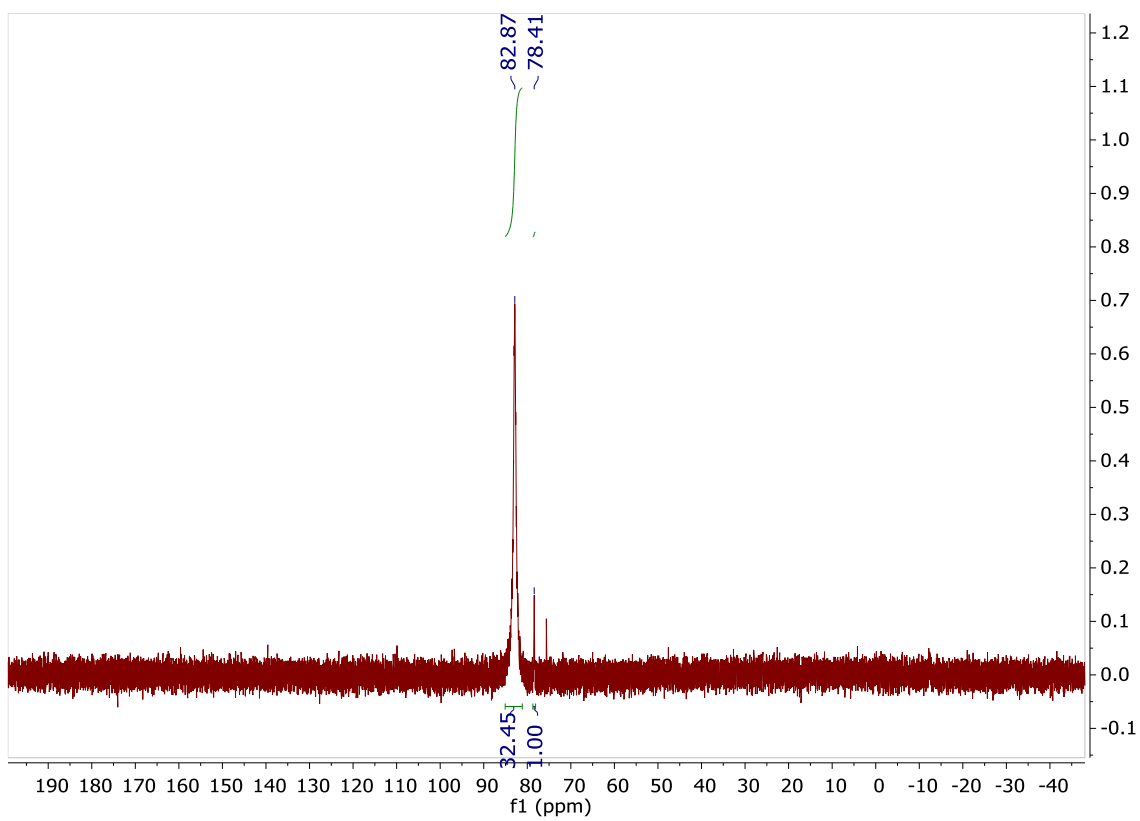


Figure S18. $^{31}\text{P}\{^1\text{H}\}$ NMR spectrum in PhF of as-synthesized **2**- ^{15}N .

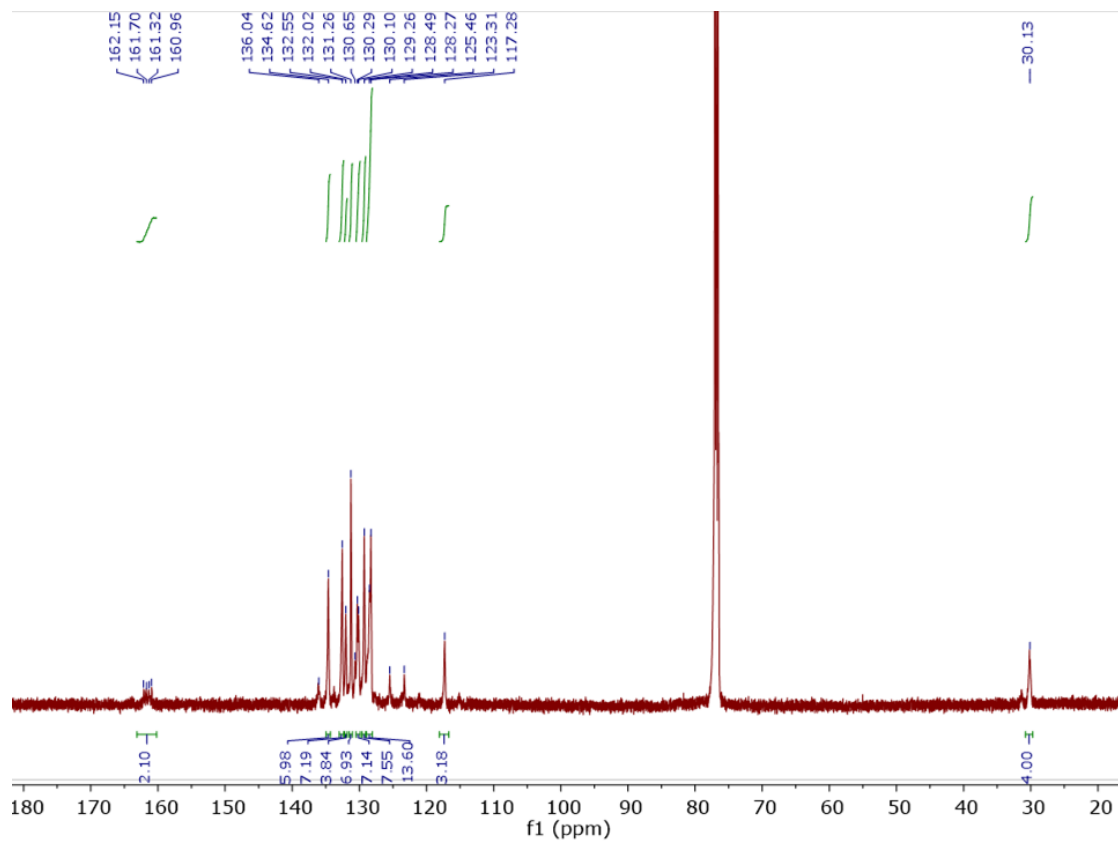


Figure S19. $^{13}\text{C}\{^1\text{H}\}$ NMR spectrum of $2\text{-}^{15}\text{N}$ in CDCl_3 .

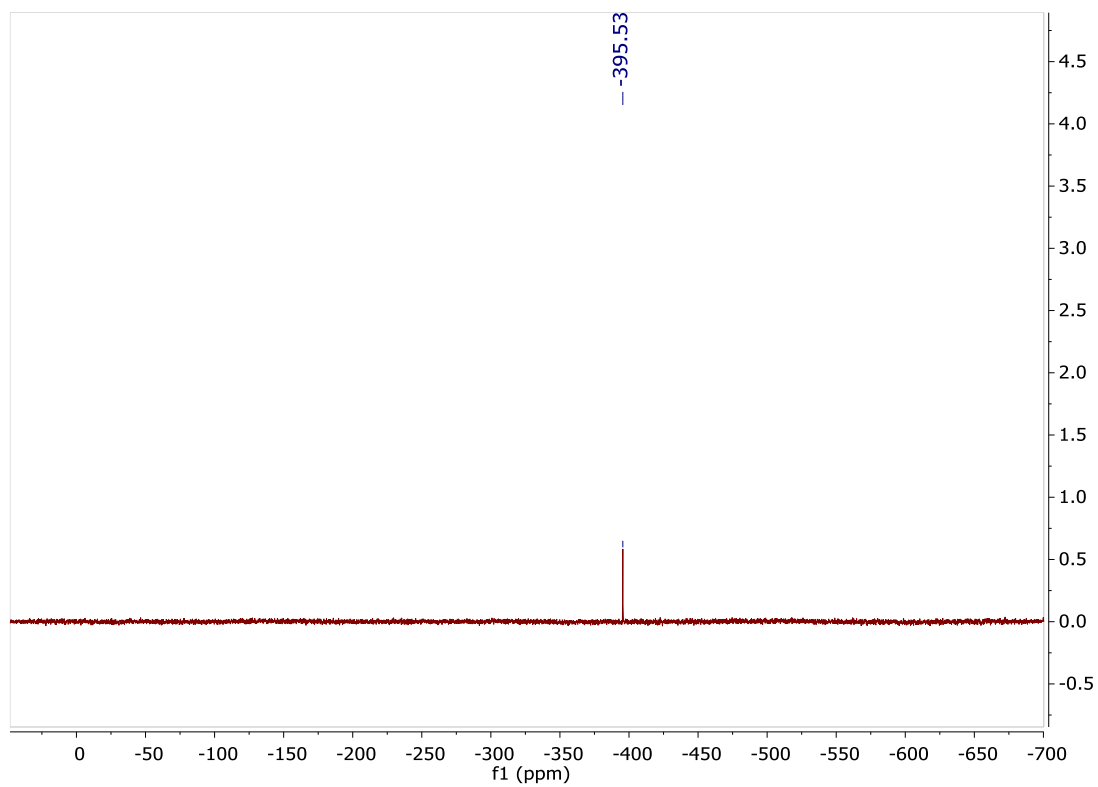


Figure S20. $^{15}\text{N}\{^1\text{H}\}$ NMR spectrum of $2\text{-}^{15}\text{N}$ in PhF.

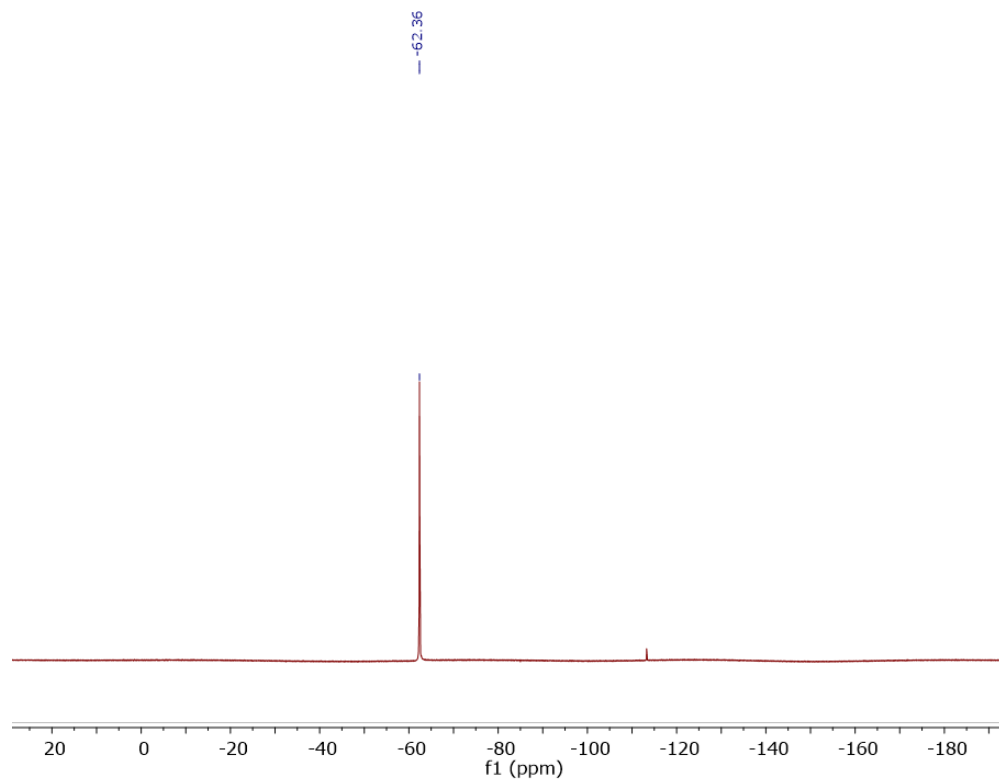


Figure S21. ^{19}F NMR spectrum of **2**- ^{15}N in CDCl_3 .

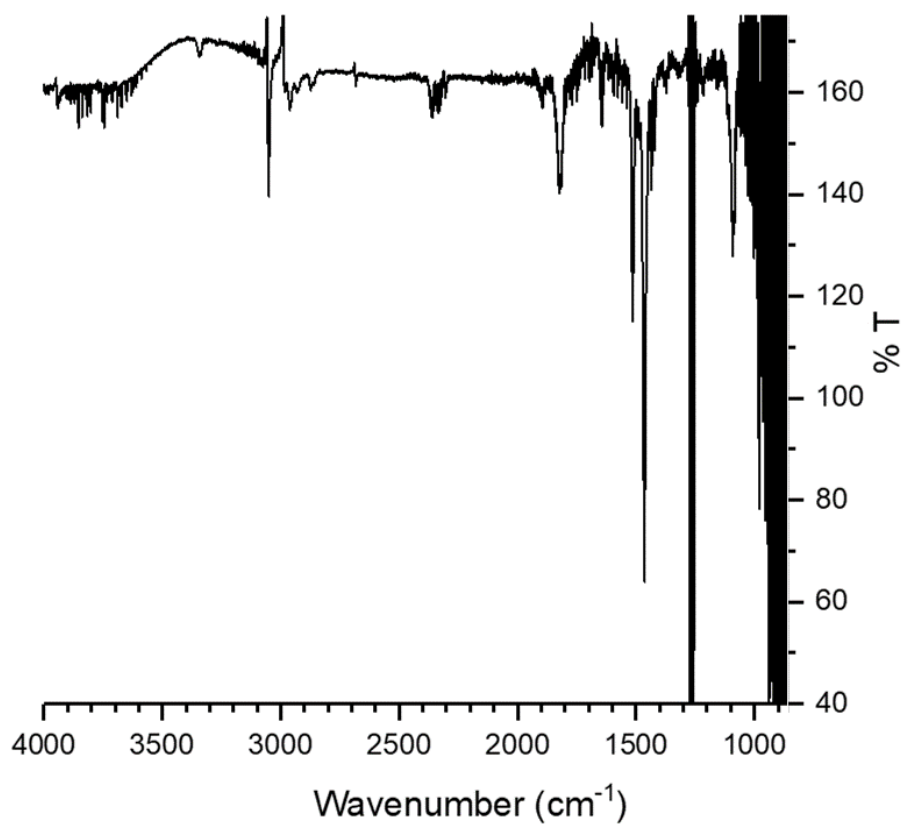


Figure S22. FT-IR spectrum of **2** in CH_2Cl_2 , with background solvent signals subtracted.

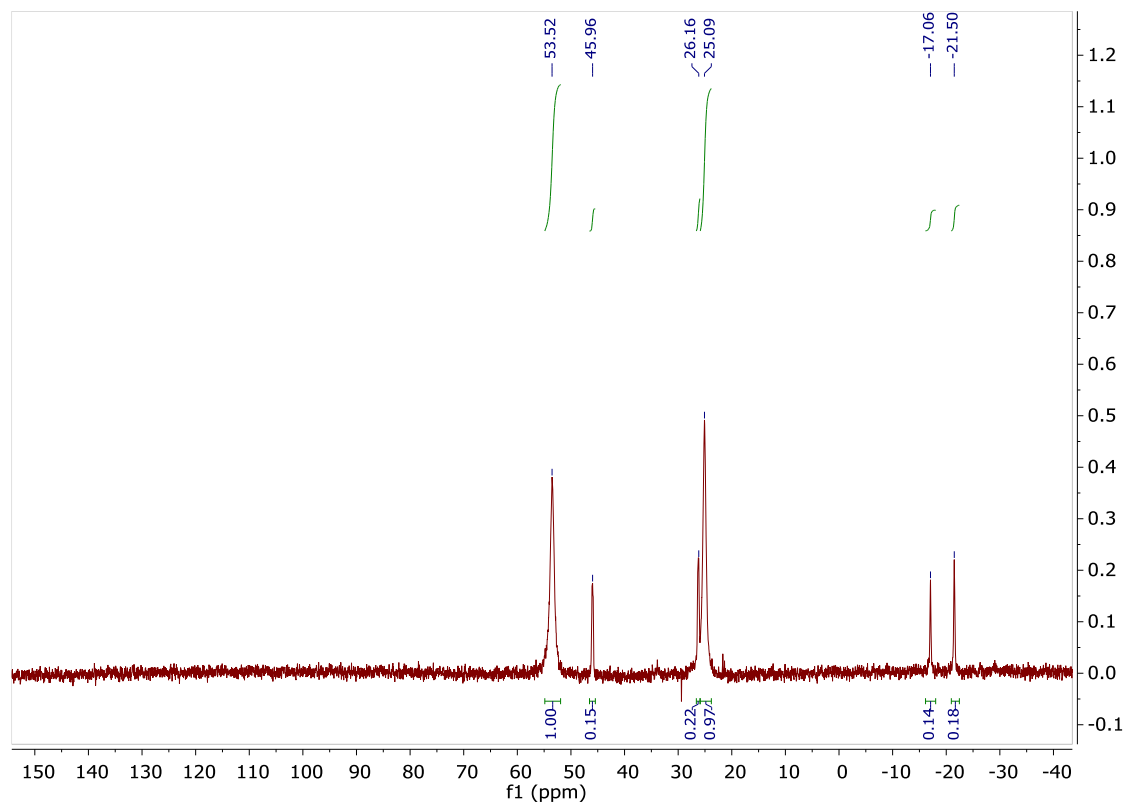


Figure S23. $^{31}\text{P}\{^1\text{H}\}$ NMR spectrum of as-synthesized $5\text{-}^{15}\text{N}$ in PhF .

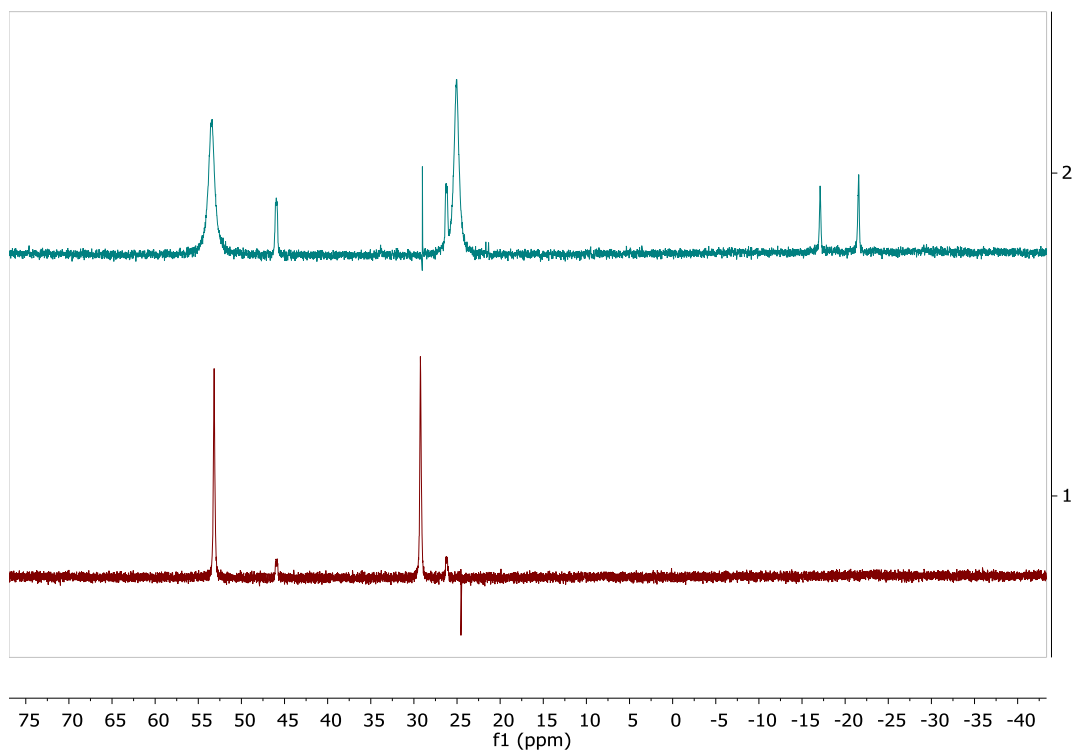


Figure S24. $^{31}\text{P}\{^1\text{H}\}$ NMR spectrum of $[\text{Mn}(\text{dppp})(\text{dppm})(\text{CO})]\text{BAr}^{\text{F}}_4$ before (bottom) and after (top) NH_3 addition.

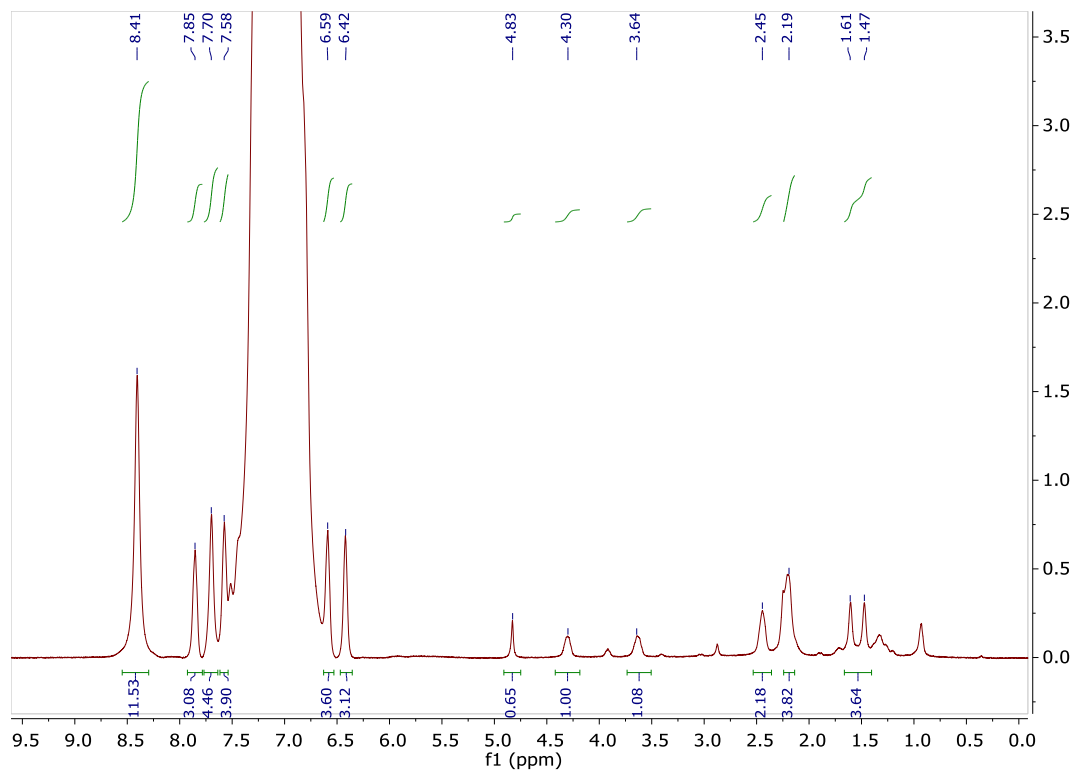


Figure S25. ^1H NMR spectrum of $5\text{-}^{15}\text{N}$ in situ after addition of $^{15}\text{NH}_3$.

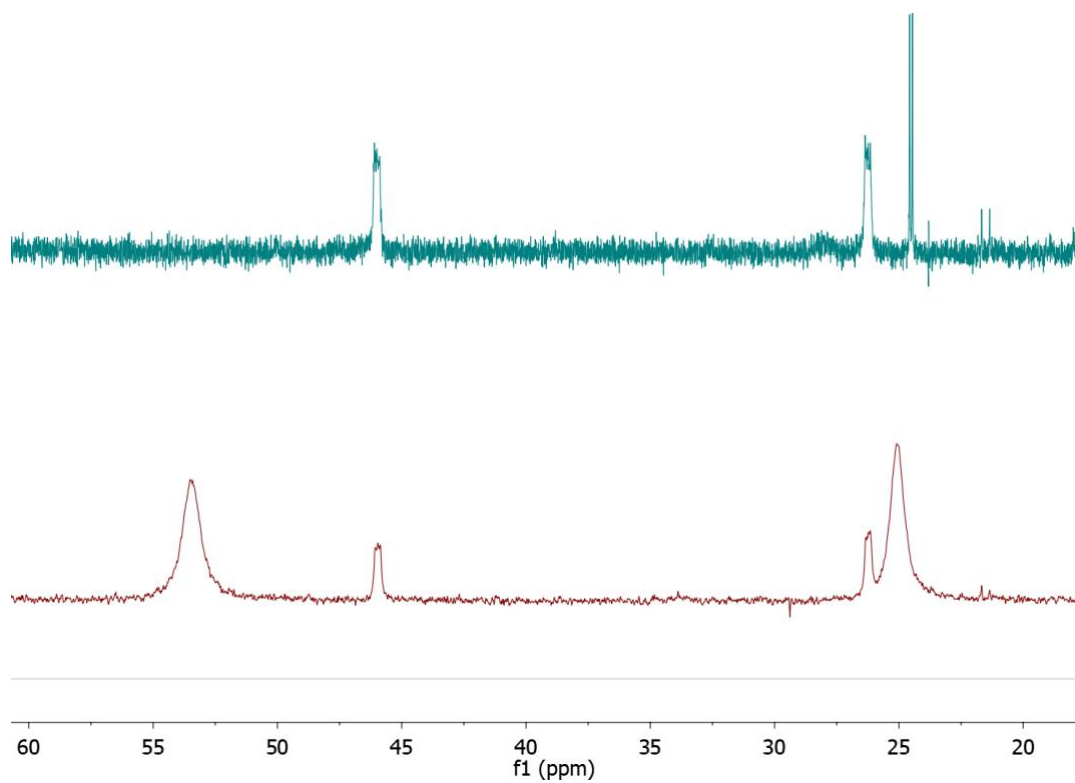


Figure S26. $^{31}\text{P}\{^1\text{H}\}$ NMR spectrum of the reaction between $5\text{-}^{15}\text{N}$ before (red) and after (blue) and 3.0 equiv. ArO^\bullet in PhF.

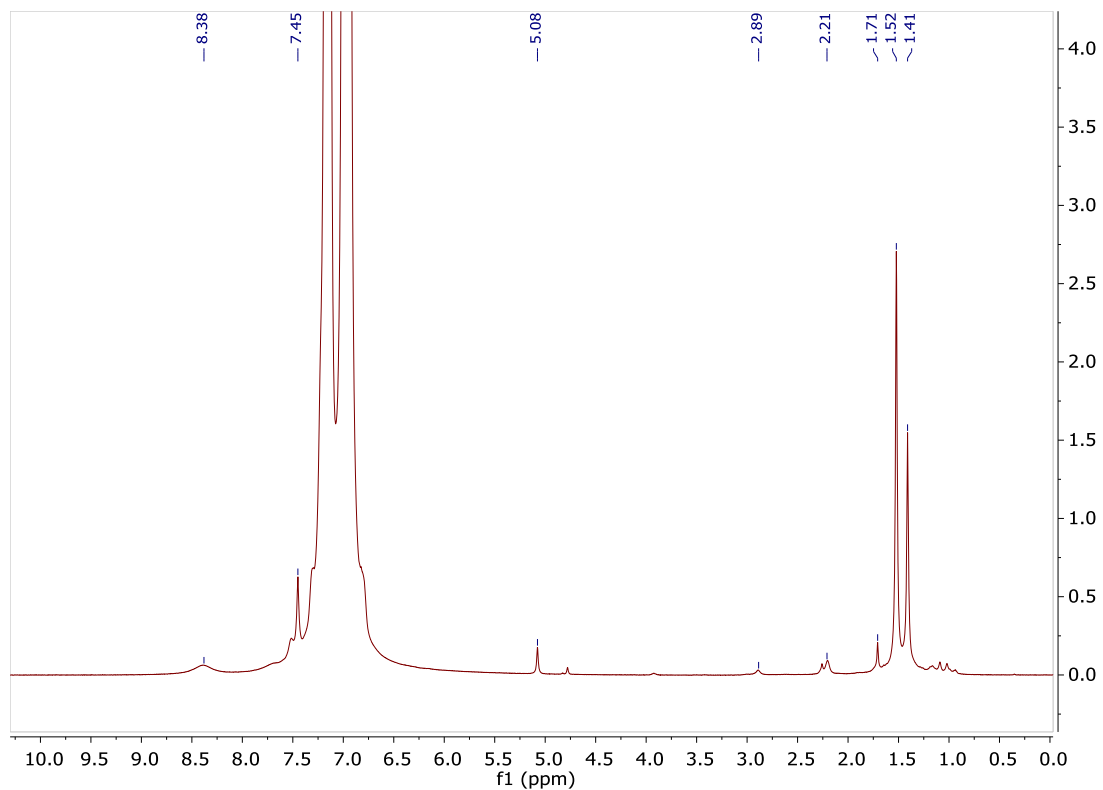


Figure S27. ^1H NMR spectrum of the reaction between $5\text{-}^{15}\text{N}$ and 3.0 equiv. ArO^\bullet recorded in PhF.

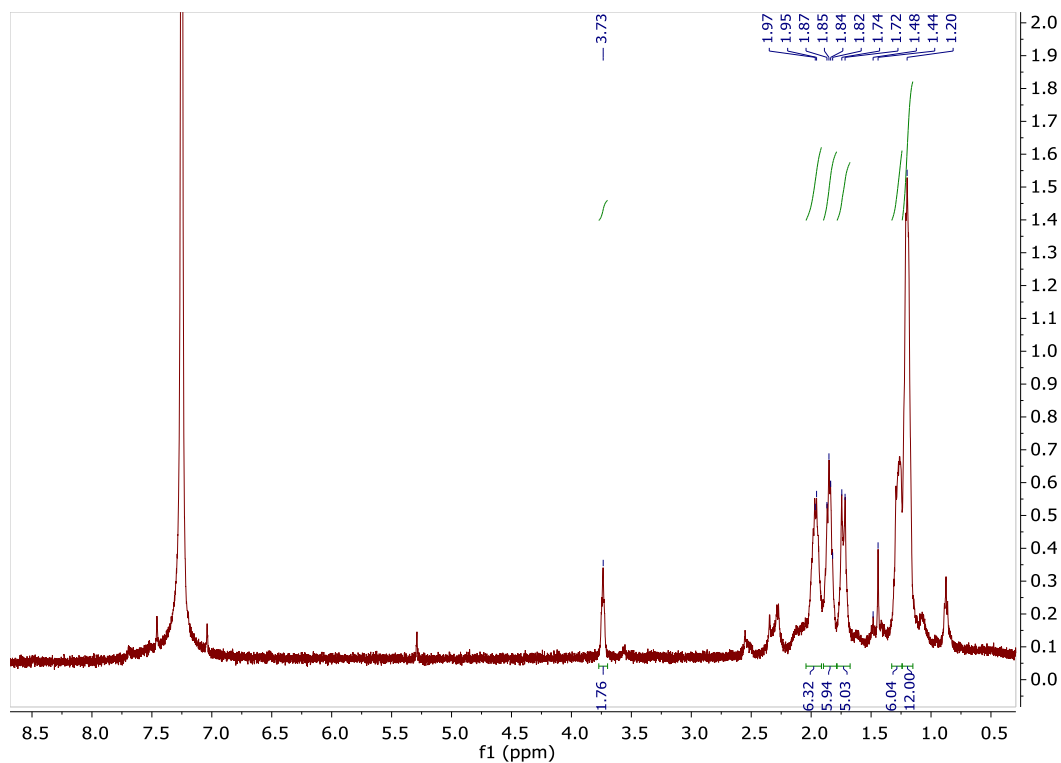


Figure S28. ^1H NMR spectrum in CDCl_3 of **3** isolated after crystallization from the reaction of **1** and 3.0 equiv. ArO^\bullet .

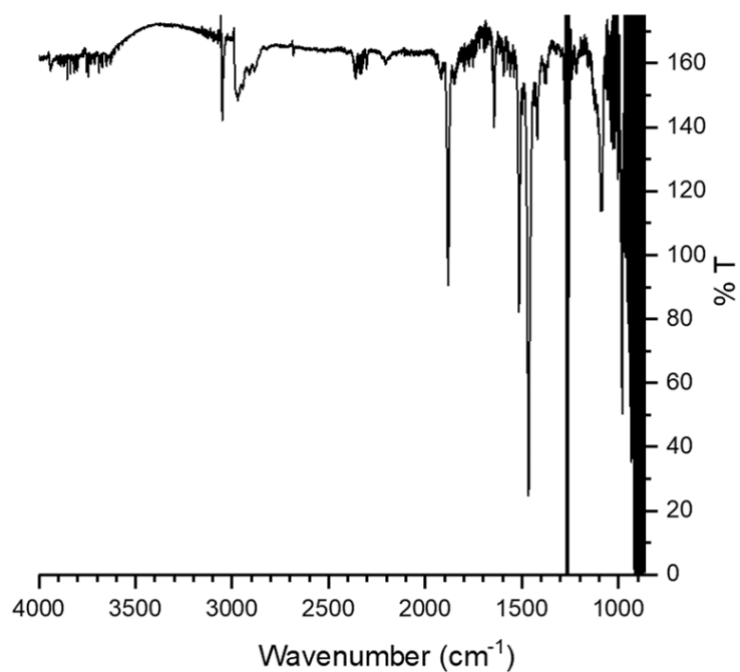


Figure S29. FT-IR spectrum of the reaction between **1** and 3 equiv. ArO• recorded in CH₂Cl₂. Background solvent signals have been subtracted.

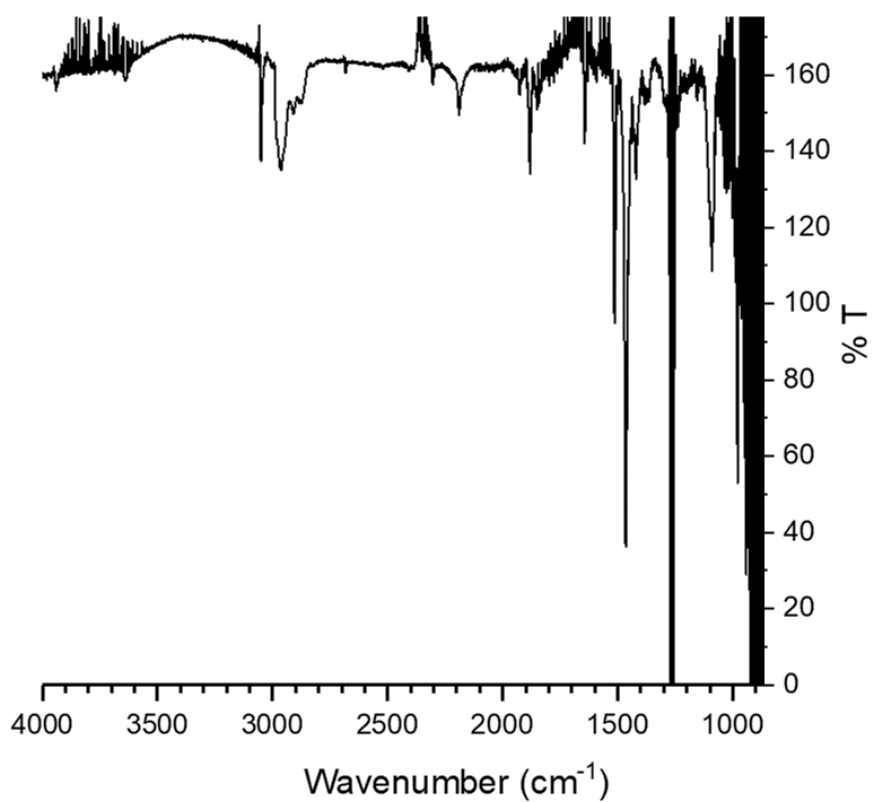


Figure S30. FT-IR spectrum of the reaction between **1**-¹⁵N and 3 equiv. ArO• recorded in CH₂Cl₂. Background solvent signals have been subtracted.

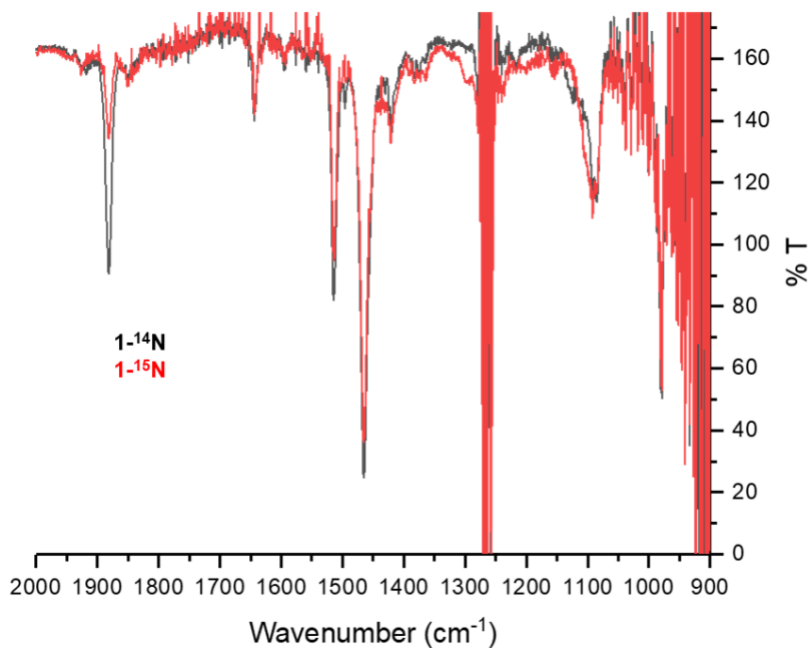


Figure S31. Overlay of the FT-IR spectra of the reactions between **1** or $1\text{-}^{15}\text{N}$ with 3.0 equiv. ArO^\bullet in CH_2Cl_2 after workup. Background solvent signals have been subtracted.

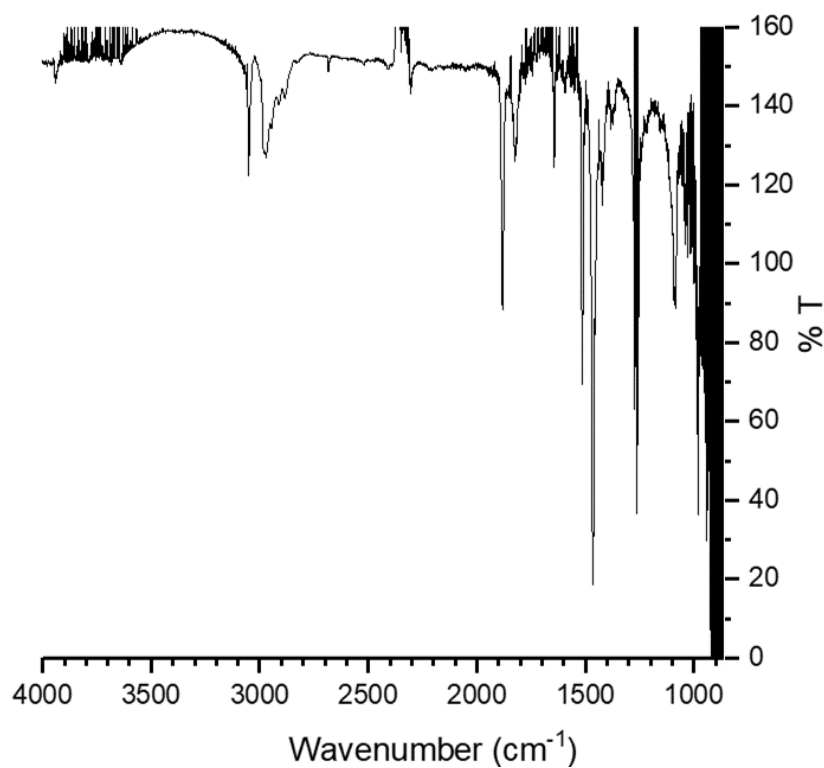


Figure S32. FT-IR spectrum of the reaction between **1** and 1.0 equiv. of ArO^\bullet recorded in CH_2Cl_2 after workup. Background solvent signals have been subtracted.

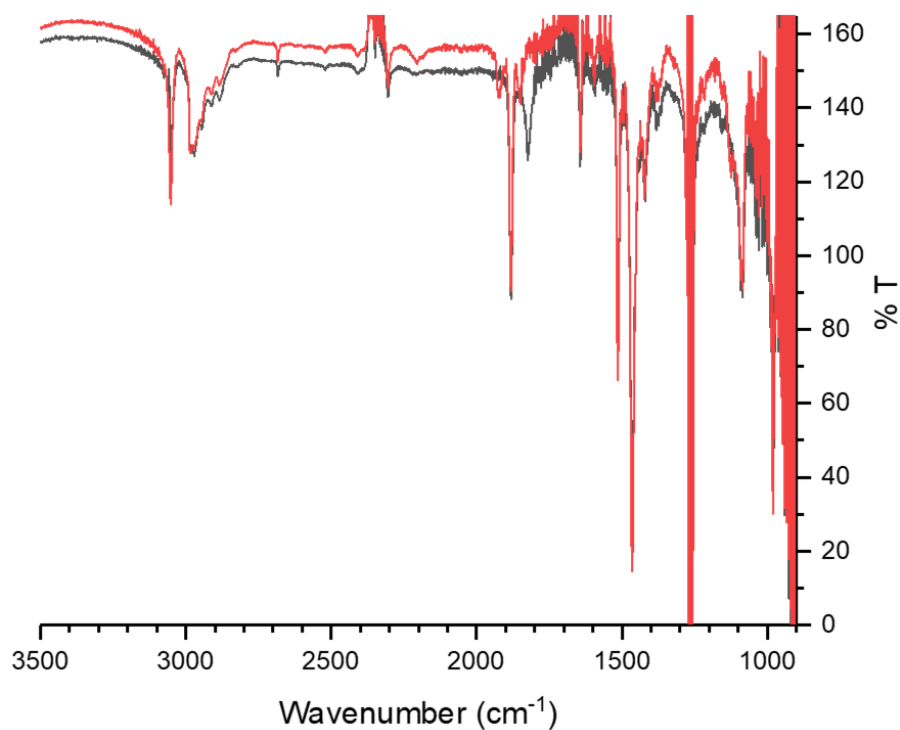


Figure S33. Overlaid FT-IR spectra of the reactions between **1** and 1.0 equiv. (black) or 3.0 equiv. (red) ArO• recorded in CH₂Cl₂ after workup. Background solvent signals have been subtracted.

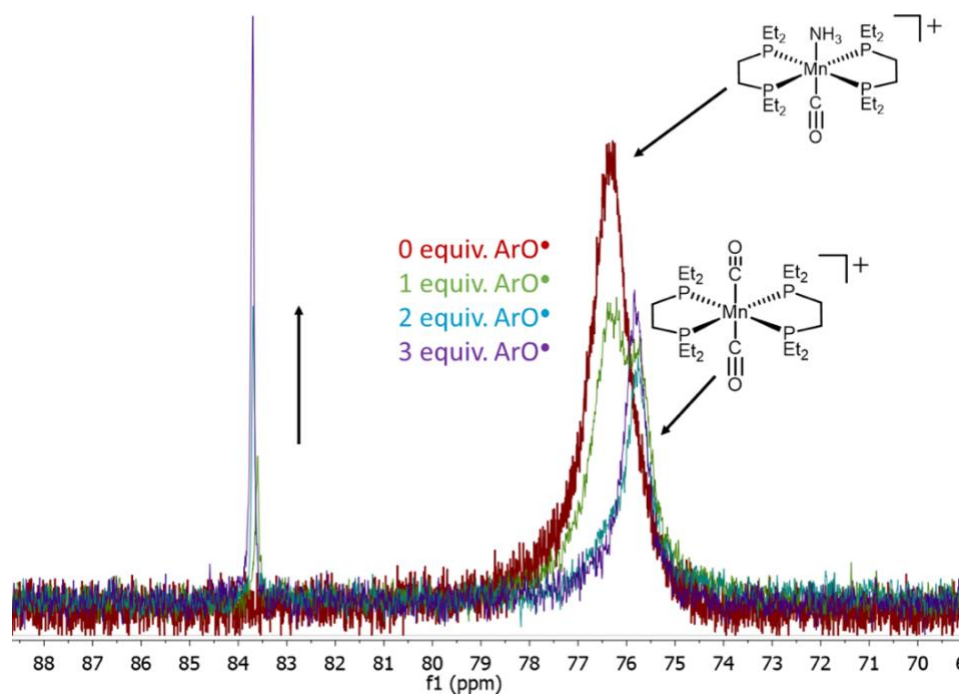


Figure S34. ³¹P{¹H} NMR spectrum of the reaction between **1** and 1, 2 and 3 sequentially added equivalents of ArO• in PhF.

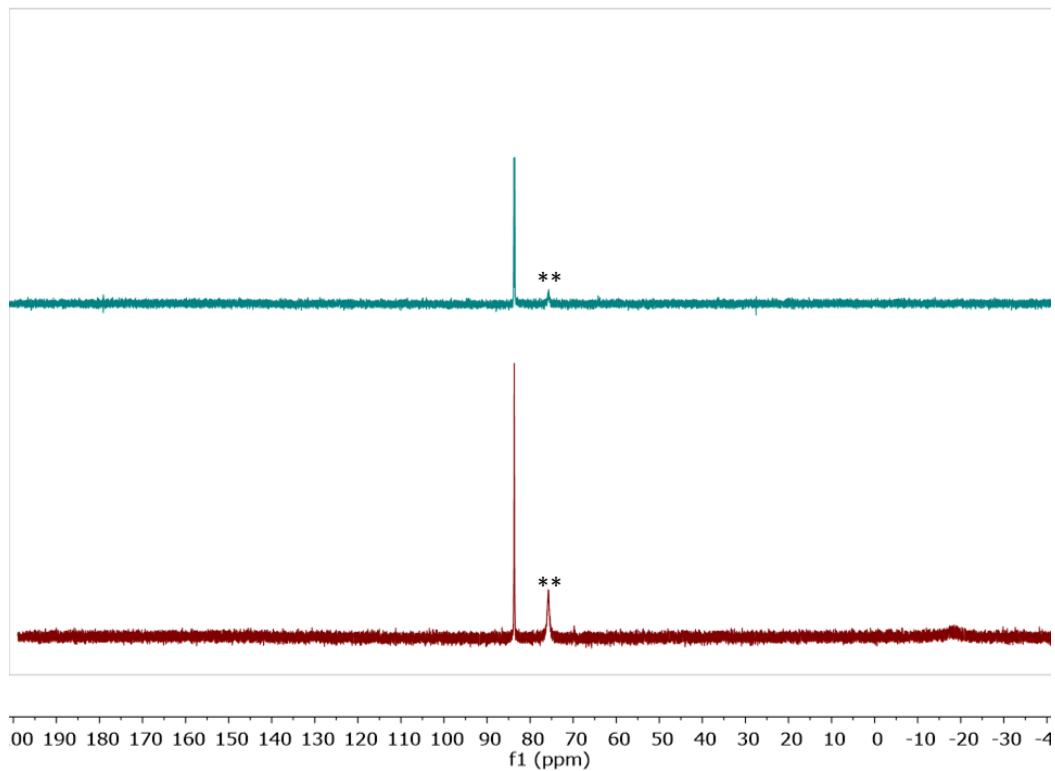


Figure S35. $^{31}\text{P}\{^1\text{H}\}$ NMR spectrum of **1** (bottom) or **1**- ^{15}N treated with 3 equiv. $\text{ArO}\bullet$ in PhF.

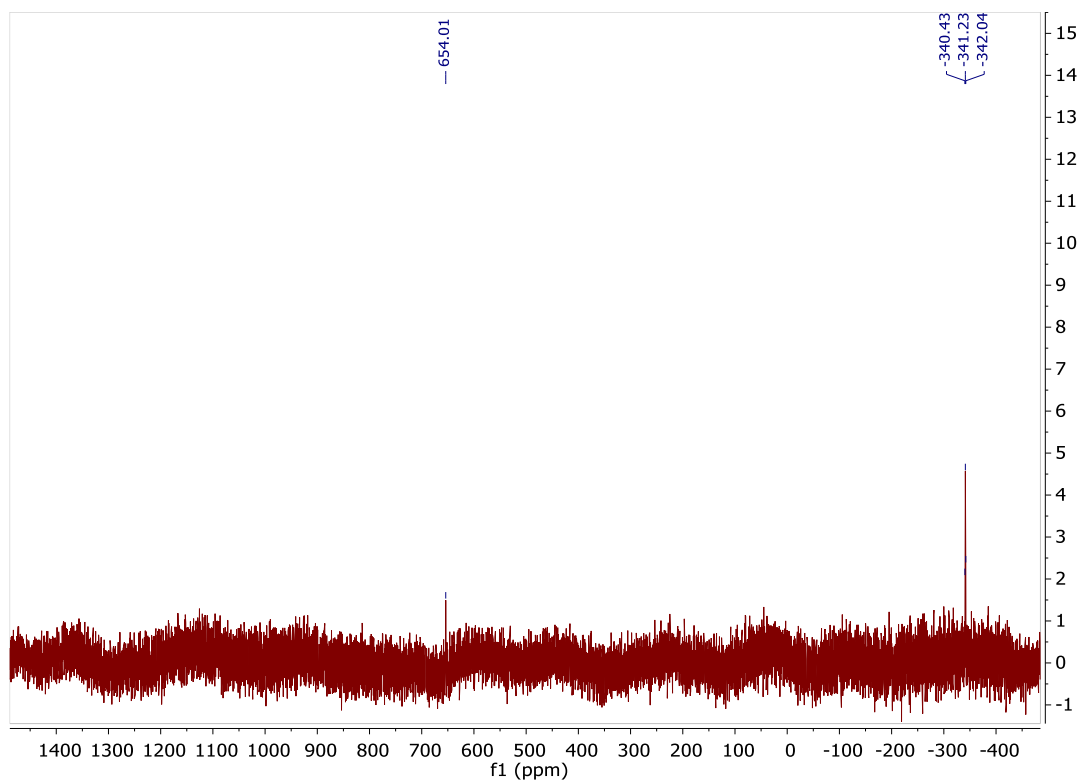


Figure S36. $^{15}\text{N}\{^1\text{H}\}$ NMR spectrum of the reaction between **1**- ^{15}N and 3 $\text{ArO}\bullet$ in PhF. NT=20,000 scans.

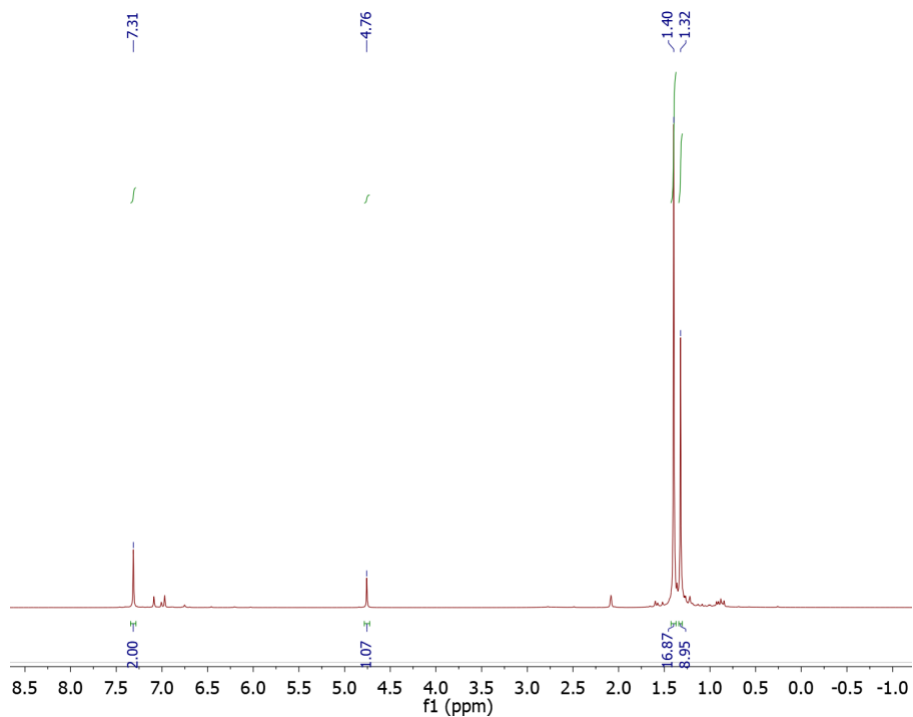


Figure S37. ^1H NMR spectrum of the pentane triturate of the reaction between **1** and 3.0 equiv. ArO^\bullet in toluene- d_8 corresponding to 2,4,6-tritertbutylphenol.

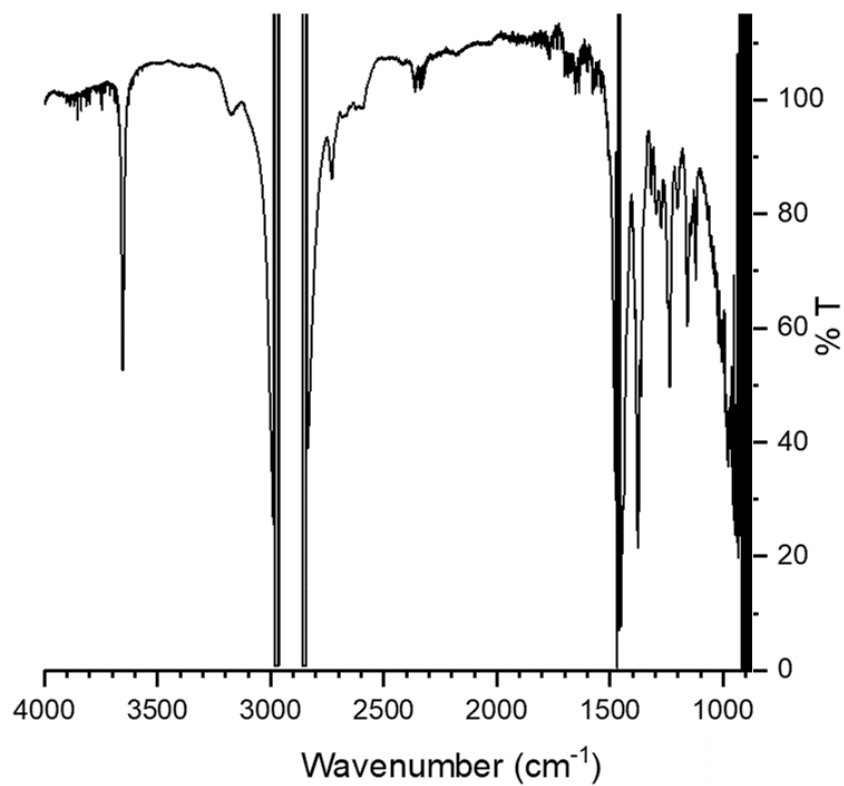


Figure S38. FT-IR spectrum of the pentane triturate of the reaction between **1** and 3.0 equiv. ArO^\bullet corresponding to 2,4,6-tritertbutylphenol in n -hexane with background solvent signals subtracted.

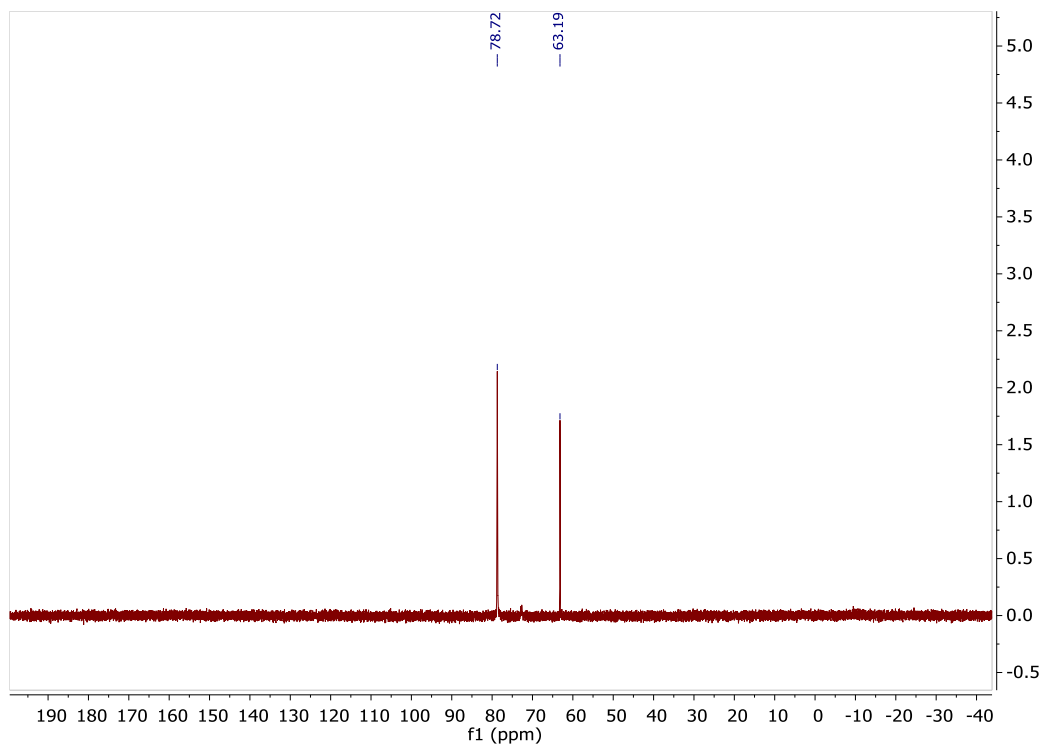


Figure S39. $^{31}\text{P}\{^1\text{H}\}$ NMR spectrum of the reaction between **2** and 3 equiv. ArO^\bullet after 72 h in PhF at room temperature.

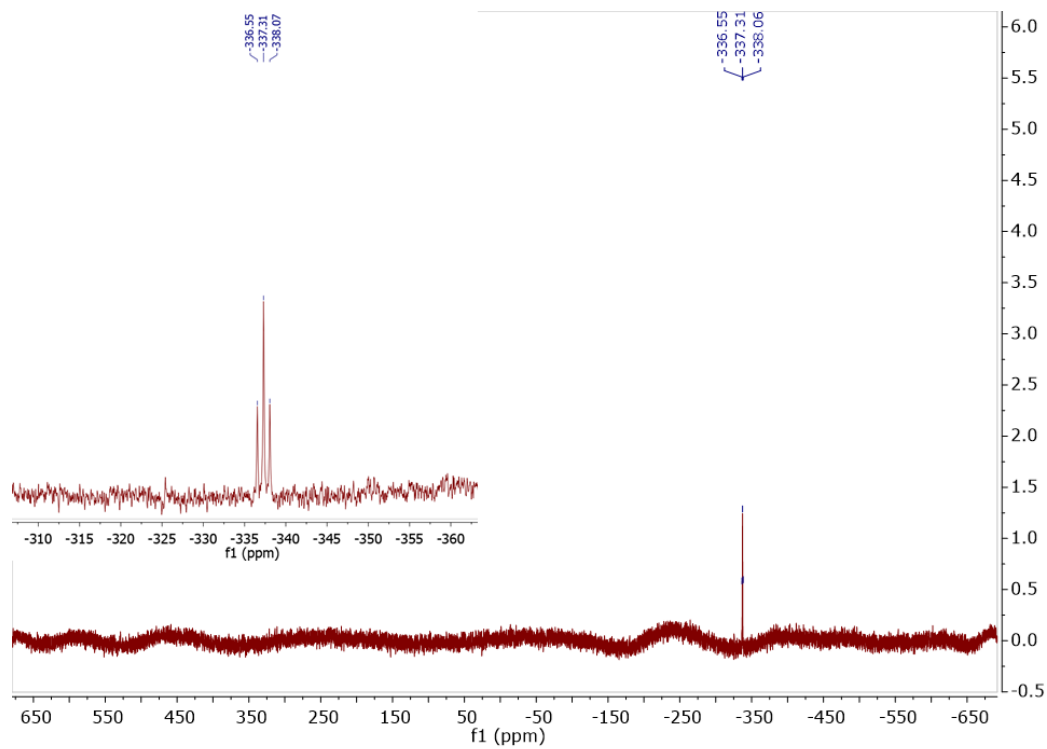


Figure S40. ^{15}N NMR spectrum of the reaction between **2**- ^{15}N and 3 equiv. ArO^\bullet in PhF at 298 K.

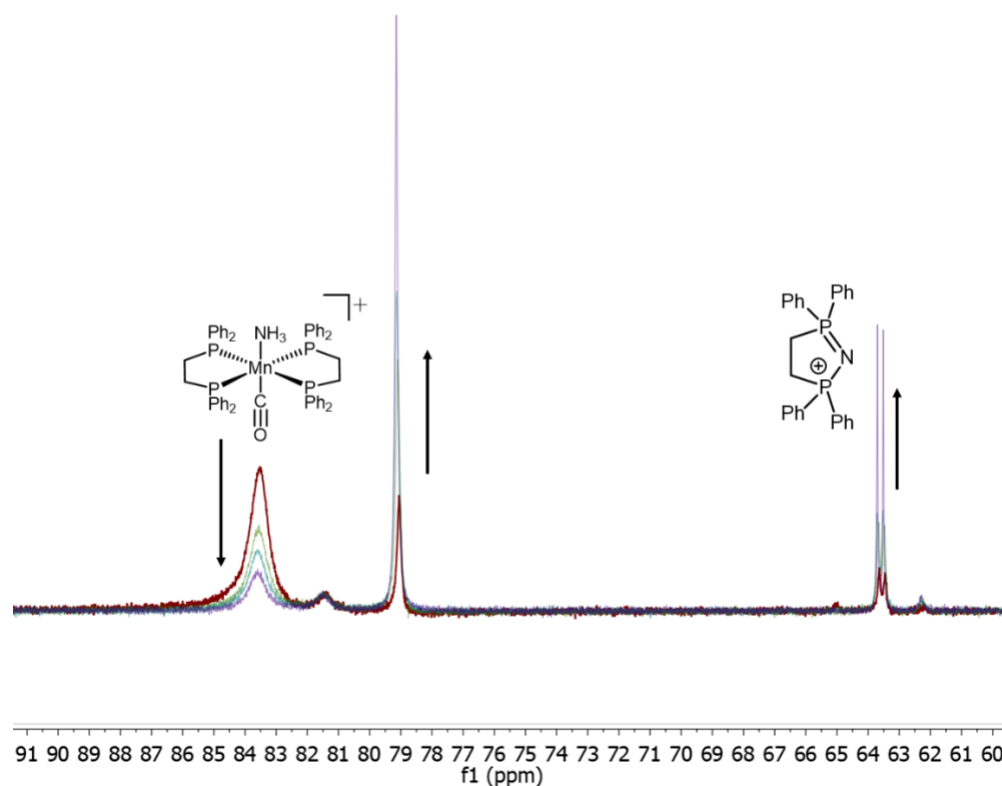


Figure S41. $^{31}\text{P}\{^1\text{H}\}$ NMR spectrum of the reaction between $2\text{-}^{15}\text{N}$ and 3 equiv. ArO^\bullet in PhF at 298 K.

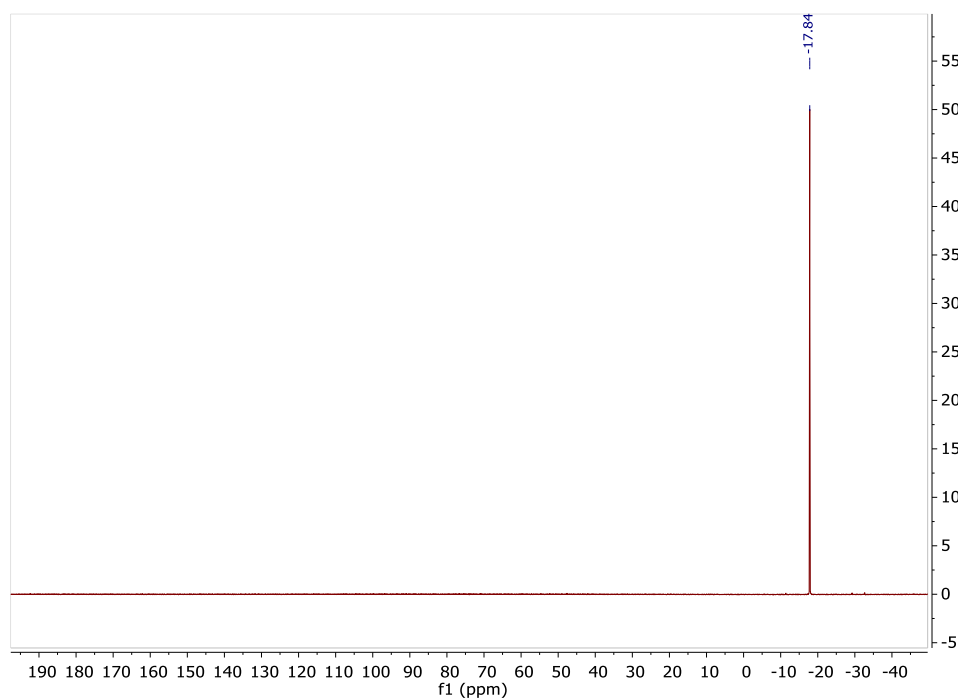


Figure S42. $^{31}\text{P}\{^1\text{H}\}$ NMR spectrum of the reaction between free depe, 4 equiv. ArO^\bullet and NH_3 in PhF after 16 h at 298K.

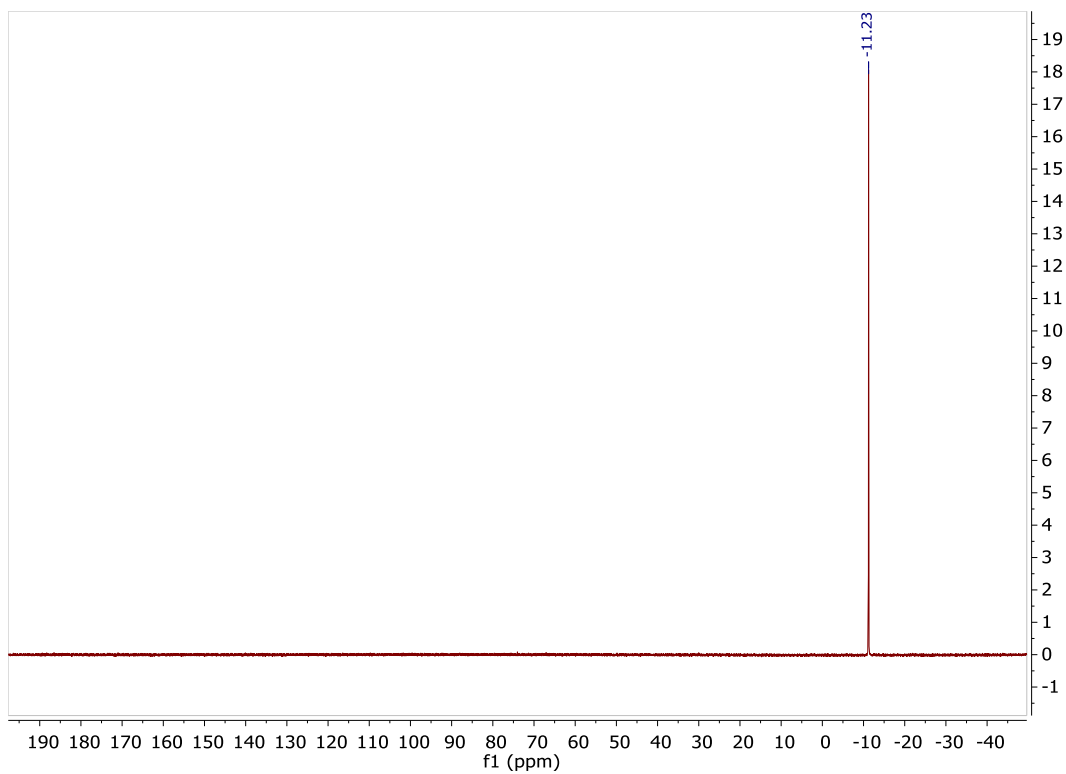


Figure S43. $^{31}\text{P}\{^1\text{H}\}$ NMR spectrum of the reaction between free dppe, 4 equiv. $\text{ArO}\bullet$ and NH_3 in PhF after 16 h at 298K.

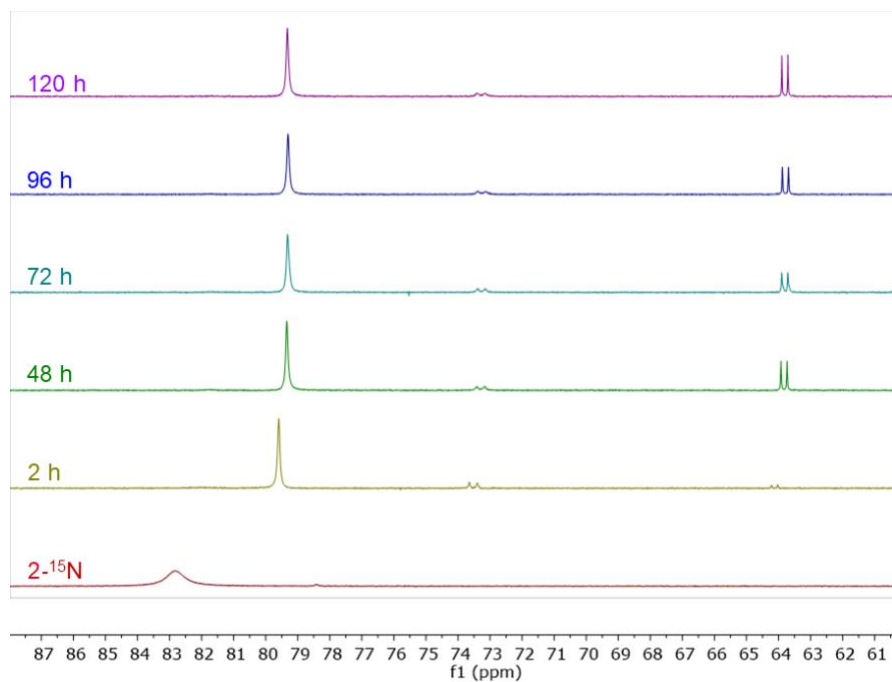


Figure S44. Time-dependence of the reaction between $2\text{-}^{15}\text{N}$ and 3 equiv. $\text{ArO}\bullet$ at 298 K in PhF. Starting Mn concentration: 38.3 mM.

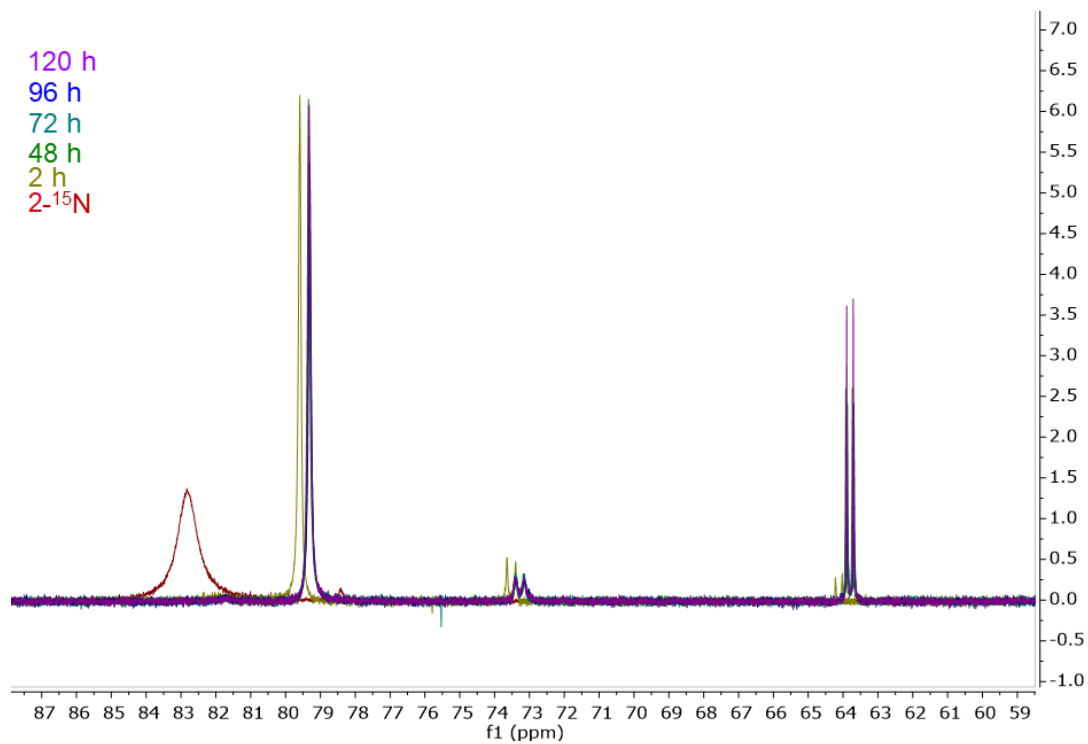


Figure S45. Superimposed time-dependence of the reaction between $2\text{-}^{15}\text{N}$ and 3 equiv. ArO^\bullet at 298 K in PhF.

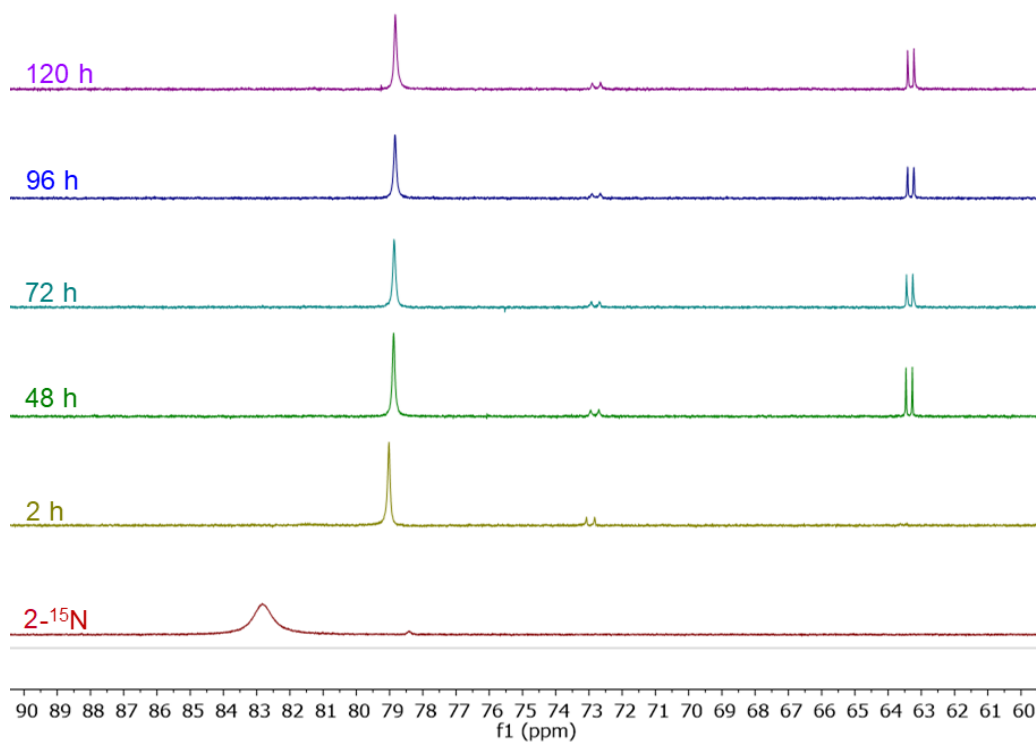


Figure S46. Time-dependence of the reaction between $2\text{-}^{15}\text{N}$ and 3 equiv. ArO^\bullet at 298 K in PhF. $[\text{Mn}]_0 = 19.6 \text{ mM}$.

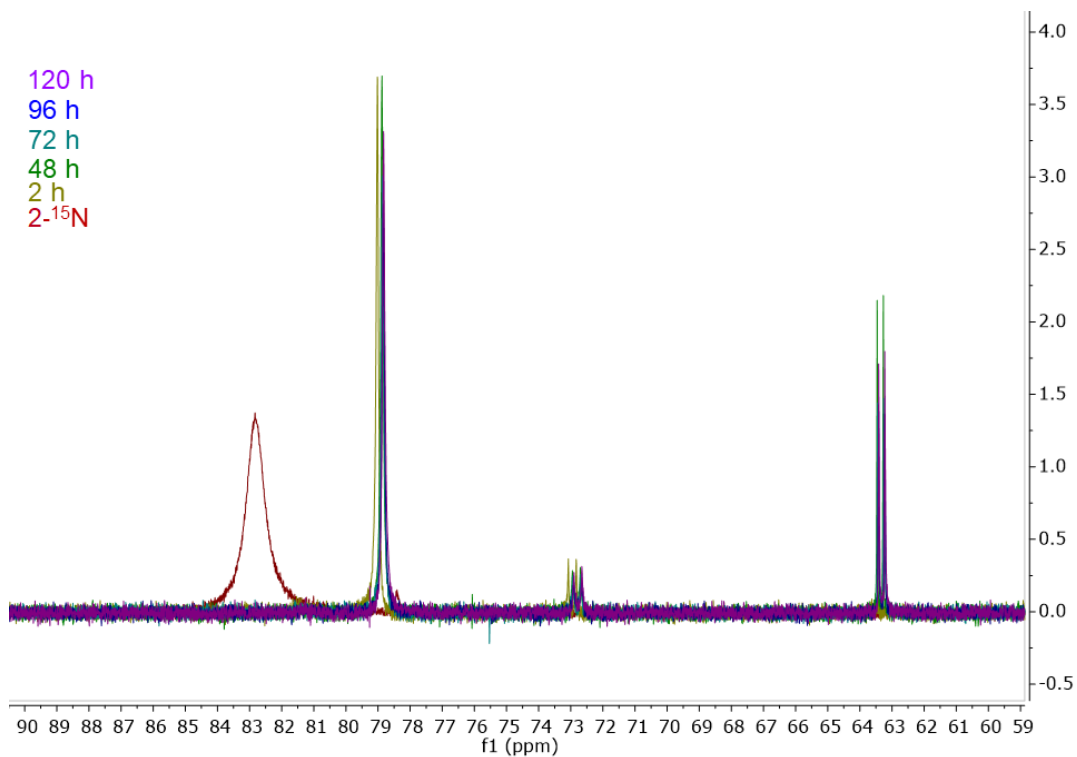


Figure S47. Superimposed time-dependence of the reaction between $2\text{-}^{15}\text{N}$ and 3 equiv. ArO^\bullet at 298 K in PhF.

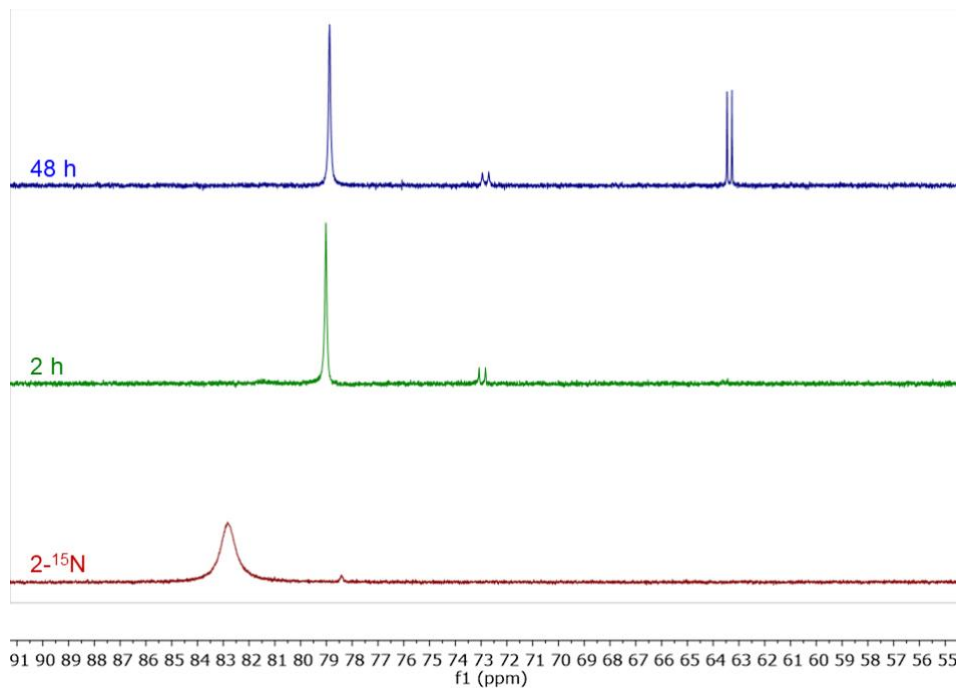


Figure S48. Time-dependence of the reaction between $2\text{-}^{15}\text{N}$ and 3 equiv. ArO^\bullet at 298 K in PhF. Starting Mn concentration: 19.6 mM.

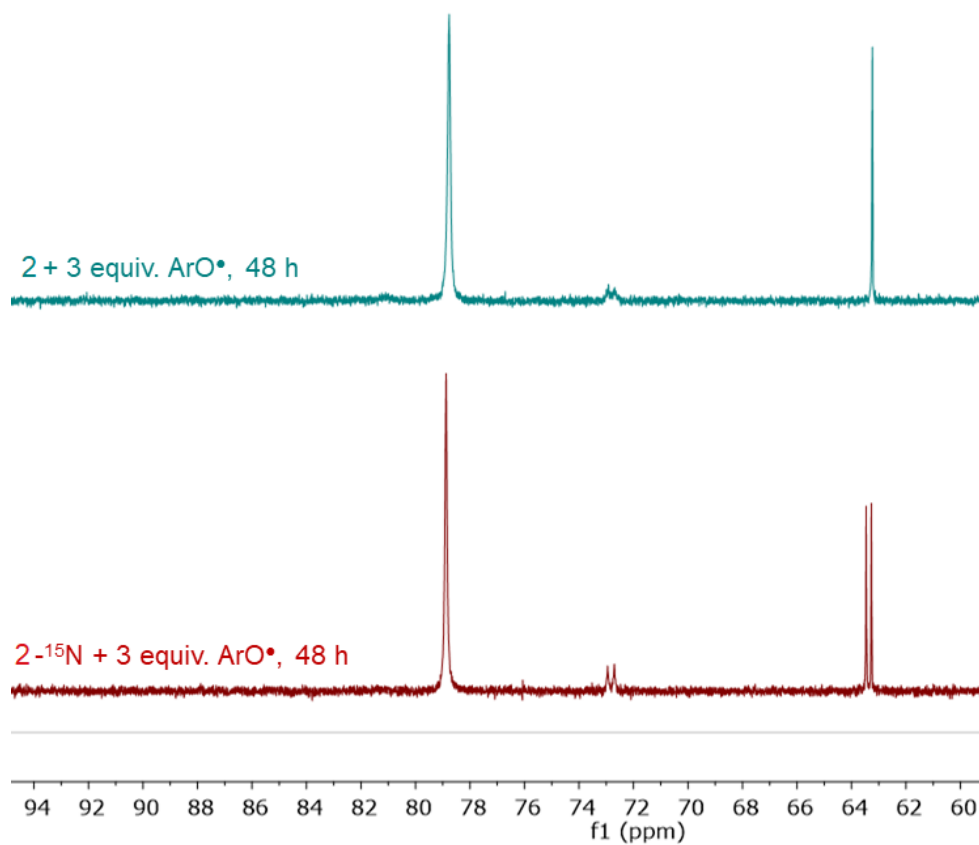


Figure S49. $^{31}\text{P}\{^1\text{H}\}$ NMR spectra of the reaction between **2** (top) or **2- ^{15}N** (bottom) with 3 equiv. ArO^\bullet in PhF.

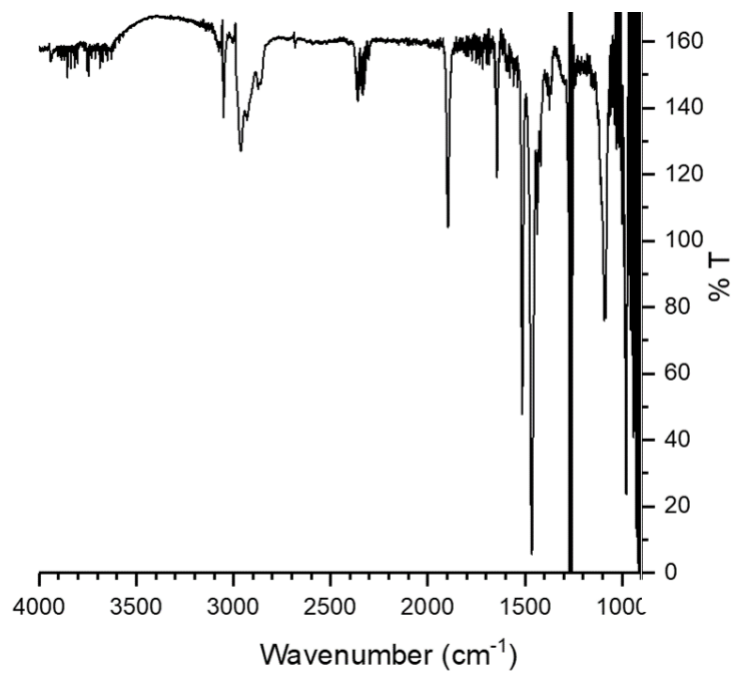


Figure S50. FT-IR spectrum of the reaction between **2** and 3.0 equiv. ArO^\bullet in CH_2Cl_2 after workup. Background solvent signals have been subtracted.

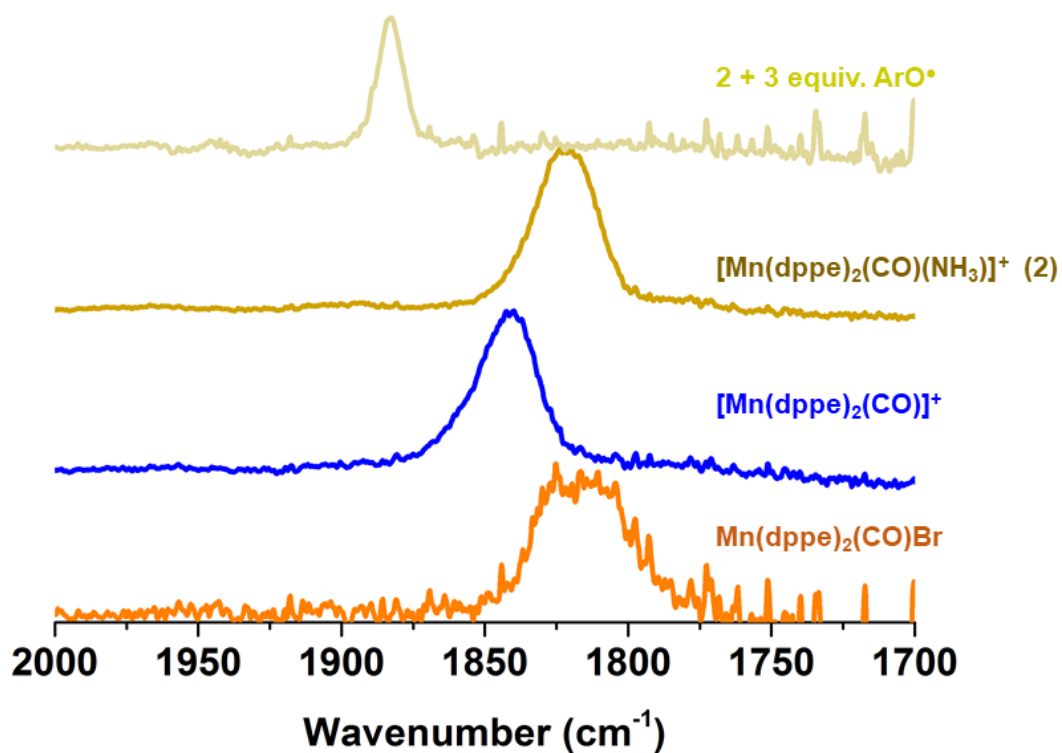


Figure S51. Comparison of IR spectra in the CO-stretching region for the overall conversion of $\text{Mn}(\text{dppe})_2(\text{CO})\text{Br}$ to **2** + 3 equiv. ArO^\bullet .

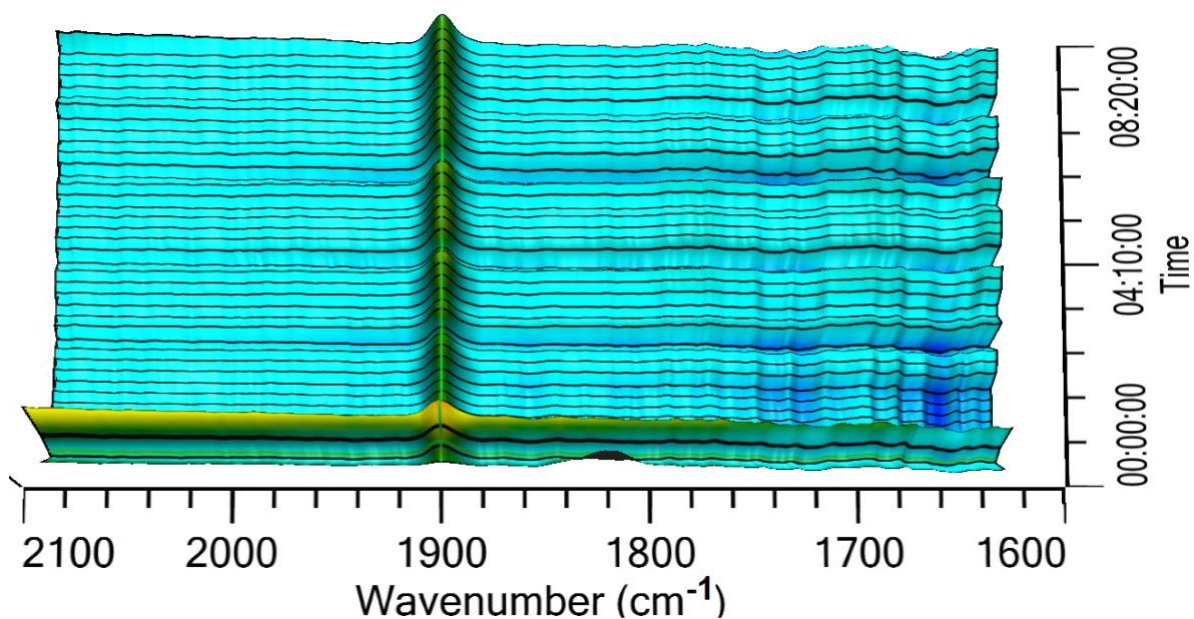


Figure S52. In situ IR spectra of the reaction between **2** and 4 equiv. ArO^\bullet in PhF to 8 h at 298 K, with emphasis on the Mn-CO region of the spectrum.

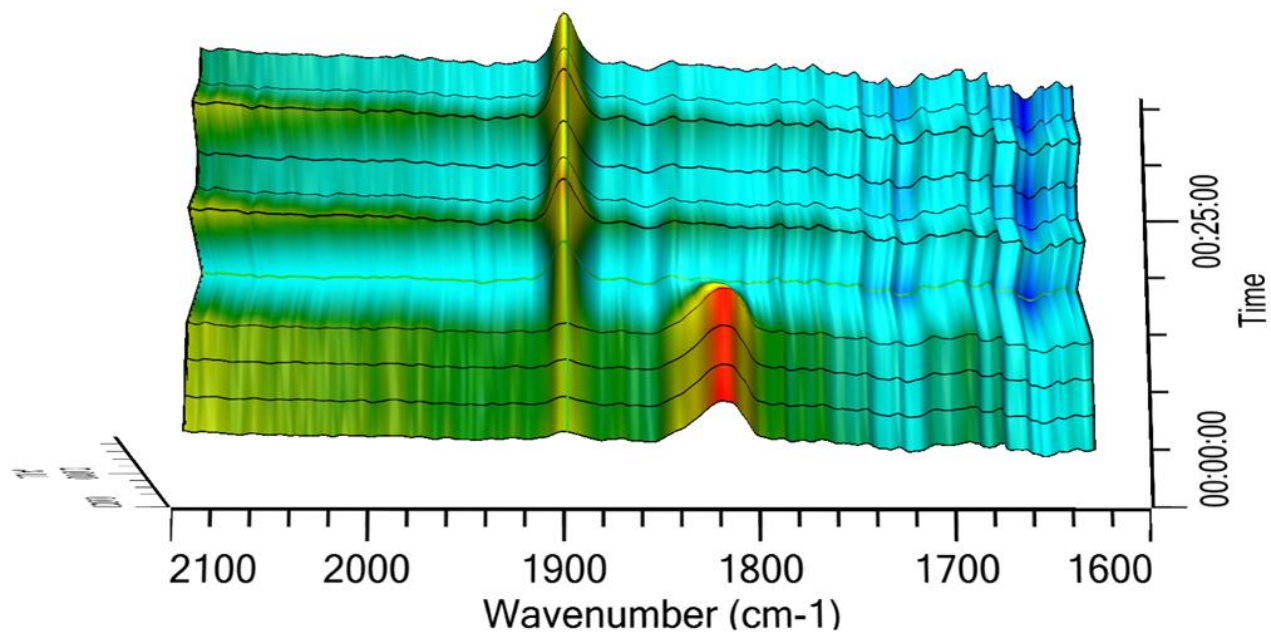


Figure S53. In situ IR spectra of the reaction between **2** and 4 equiv. ArO• in PhF out to 24 min at 298 K, with emphasis on the Mn-CO region of the spectrum.

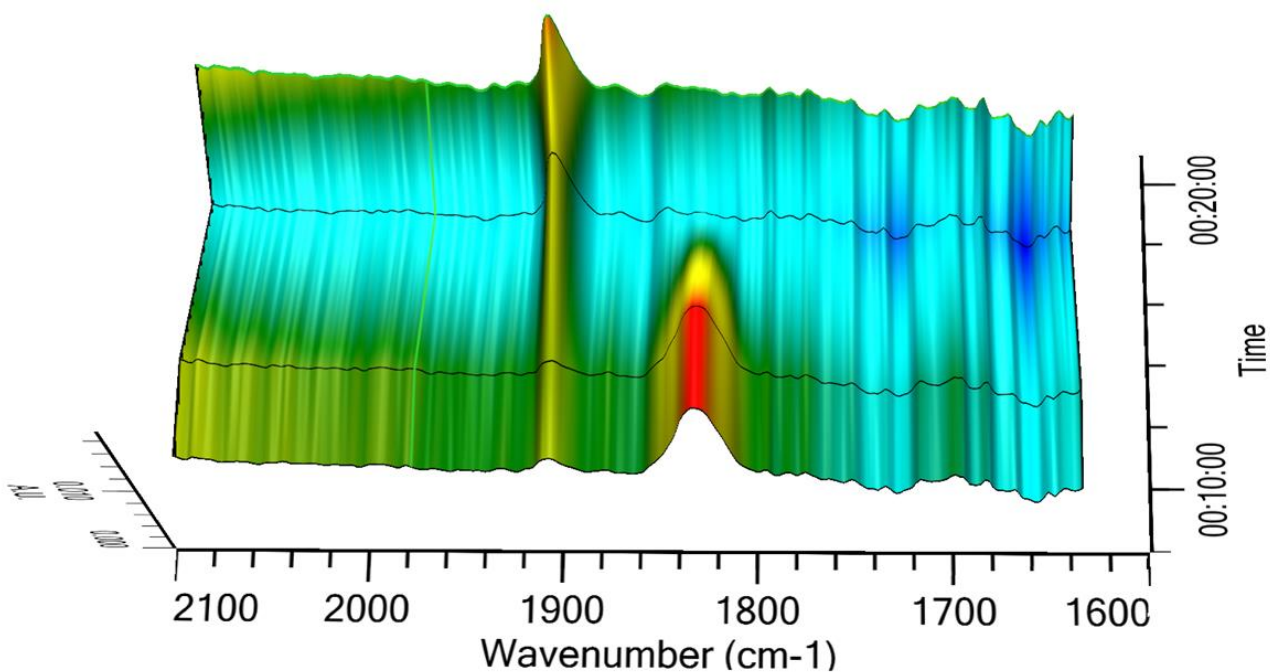


Figure S54. In situ IR spectra of the reaction between **2** and 4 equiv. ArO• in PhF upon mixing at 298 K, with emphasis on the Mn-CO region of the spectrum.

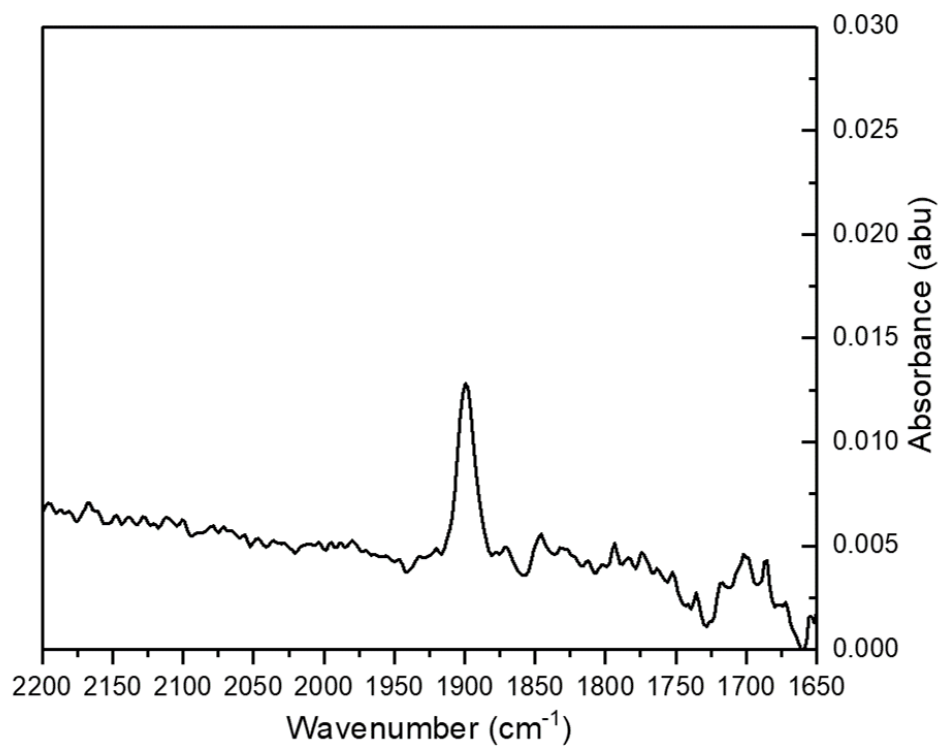


Figure S55. In situ IR spectrum of the reaction between **2** and 4 equiv. ArO[•] recorded in PhF at 5 min after mixing.

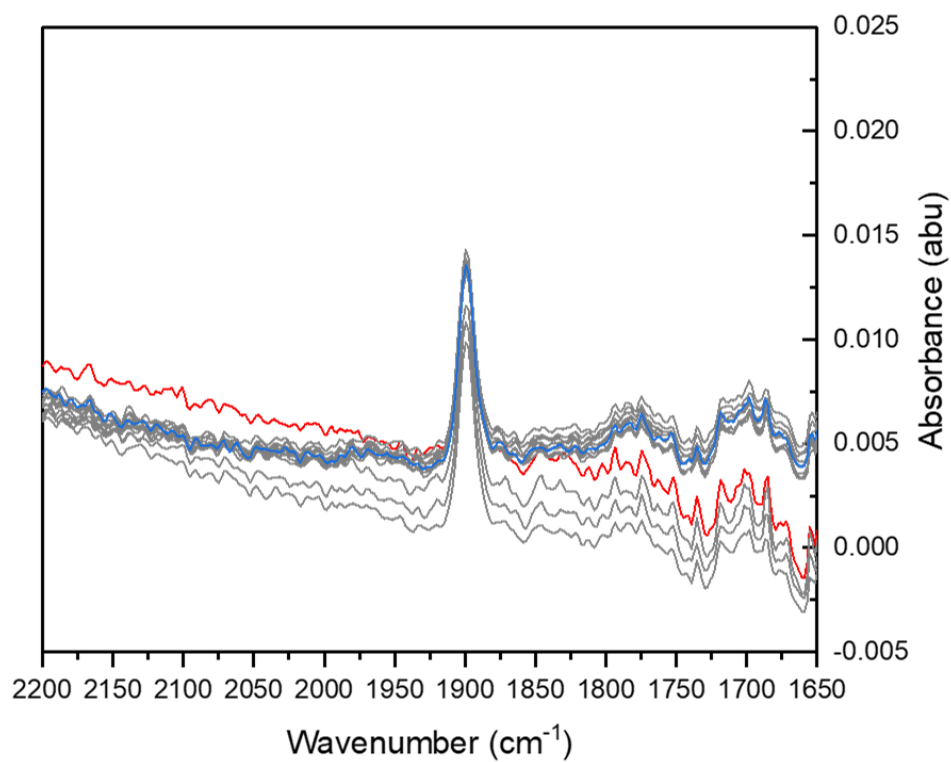


Figure S56. In situ IR spectra of the reaction between **2** and 4 equiv. ArO[•], showing spectra evolution between 48 (red) and 460 min (blue) recorded in PhF.

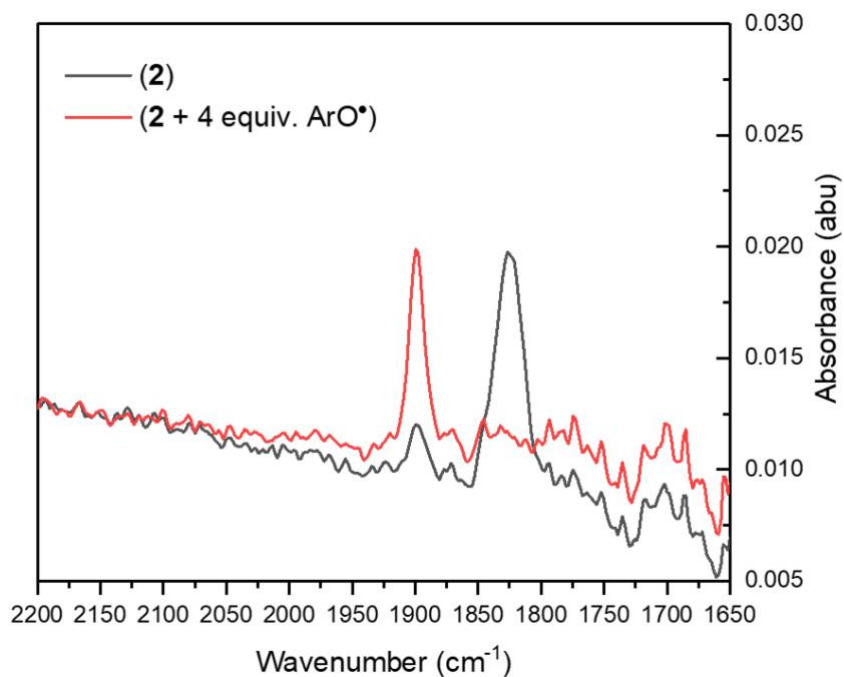


Figure S57. In situ IR spectra of the reaction between **2** and 4 equiv. ArO• in PhF, comparing **2** with product spectrum after 27 min at 298 K.

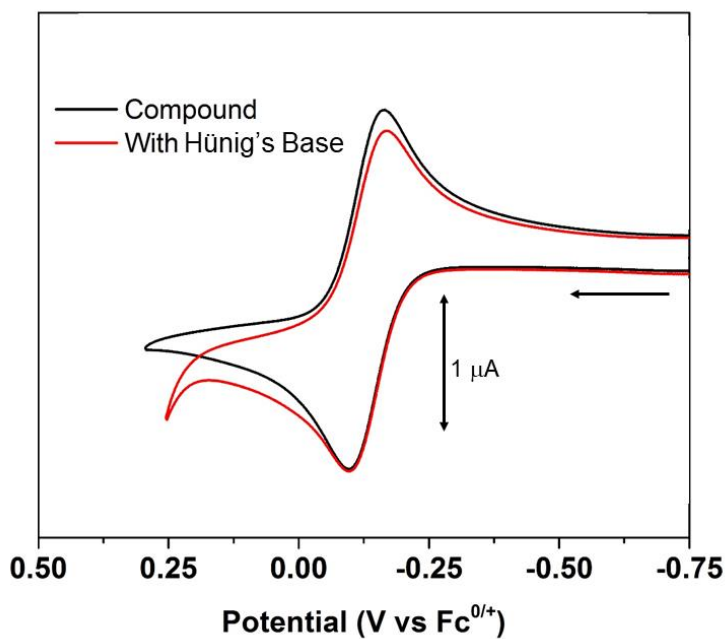


Figure S58. Cyclic voltammetry of **1** at 50 mV/s with and without exogenous base. Arrows indicate sweep origin and current scale. 0.1 M [Bu₄N]B(C₆F₅)₄ in PhF.

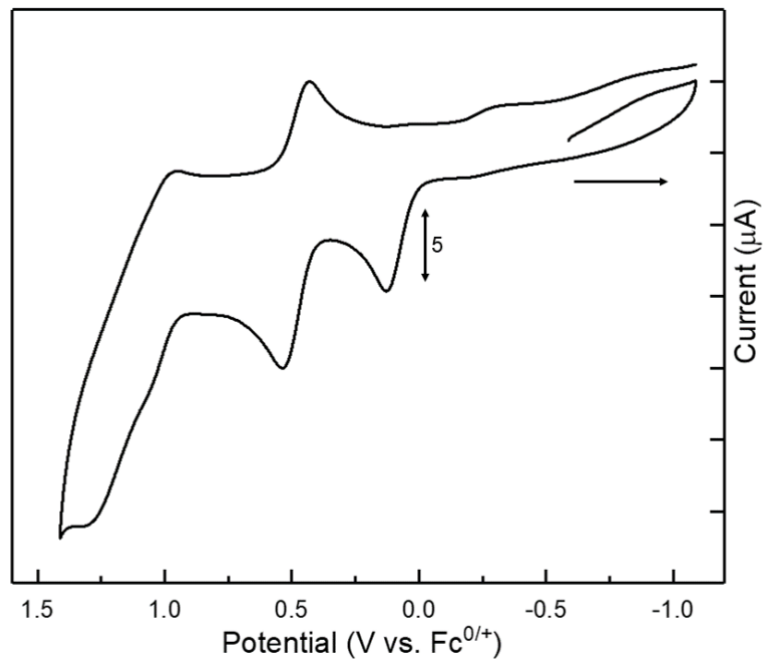


Figure S59. Cyclic voltammetry of **2** at 100 mV/s. Arrows indicate sweep origin and current scale. 0.2 M [Bu₄N]B(C₆F₅)₄ in PhF.

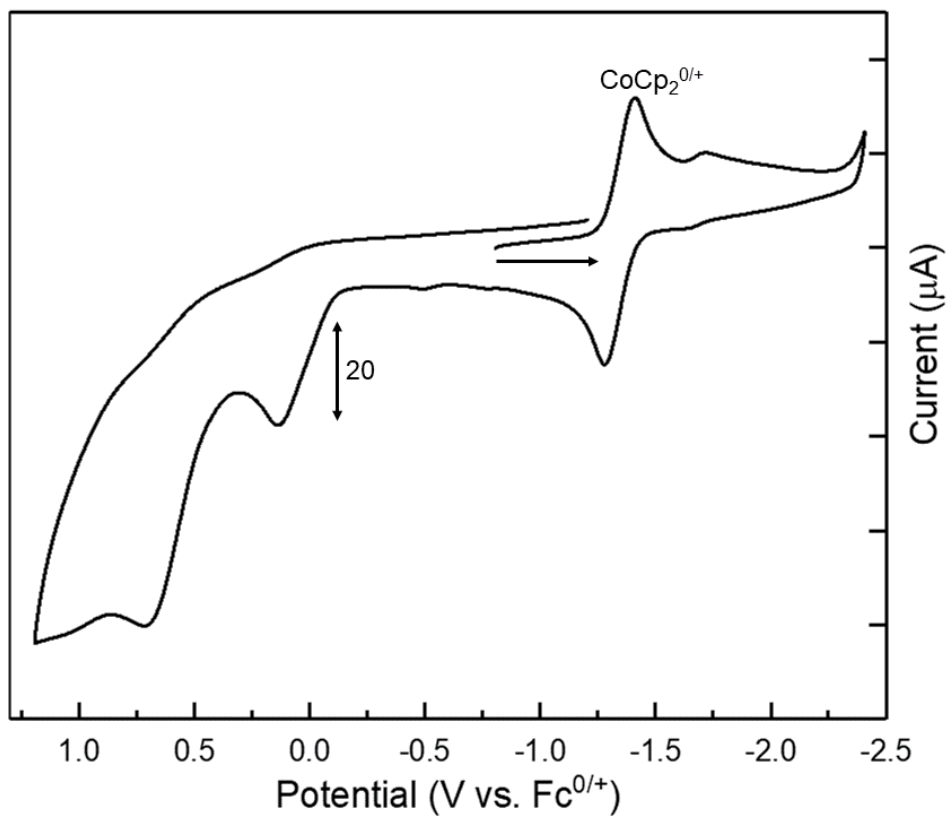


Figure S60. Cyclic voltammetry of **2** (2.0 mM) at 100 mV/s with 5 equiv. DBU added into the cell. Arrows show sweep origin and current scale. 0.2 M [Bu₄N]B(C₆F₅)₄ in PhF.

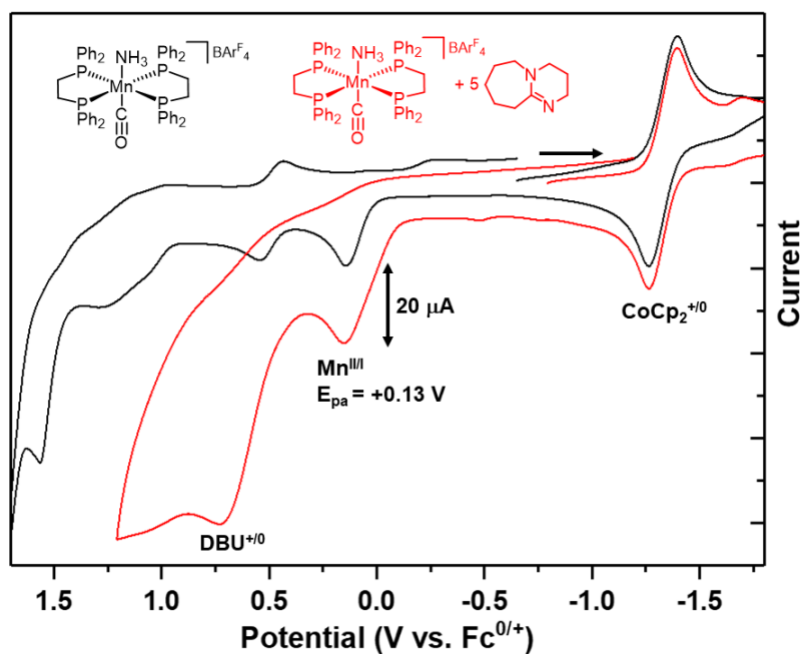


Figure S61. Overlaid cyclic voltammograms of **2** (2.0 mM) at 100 mV/s and with 5 equiv. DBU added into the cell. Arrows show sweep origin and current scale. 0.2 M $[\text{Bu}_4\text{N}]\text{B}(\text{C}_6\text{F}_5)_4$ in PhF.

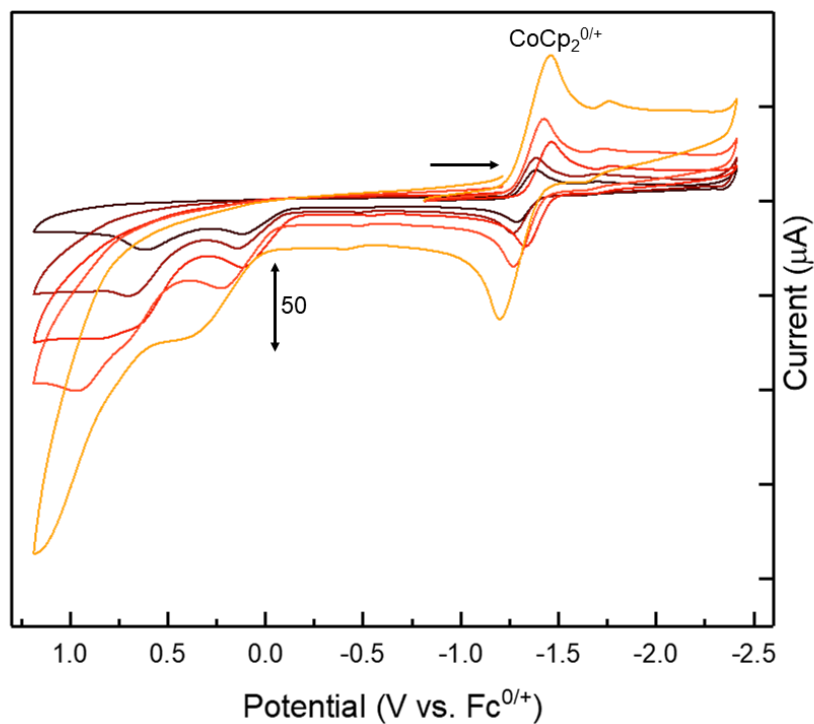


Figure S62. Cyclic voltammetry of **2** (2.0 mM) with 5 equiv. DBU at different scan rates (25-800 mV/s). Arrows indicate sweep origin and current scale. 0.2 M $[\text{Bu}_4\text{N}]\text{B}(\text{C}_6\text{F}_5)_4$ in PhF.

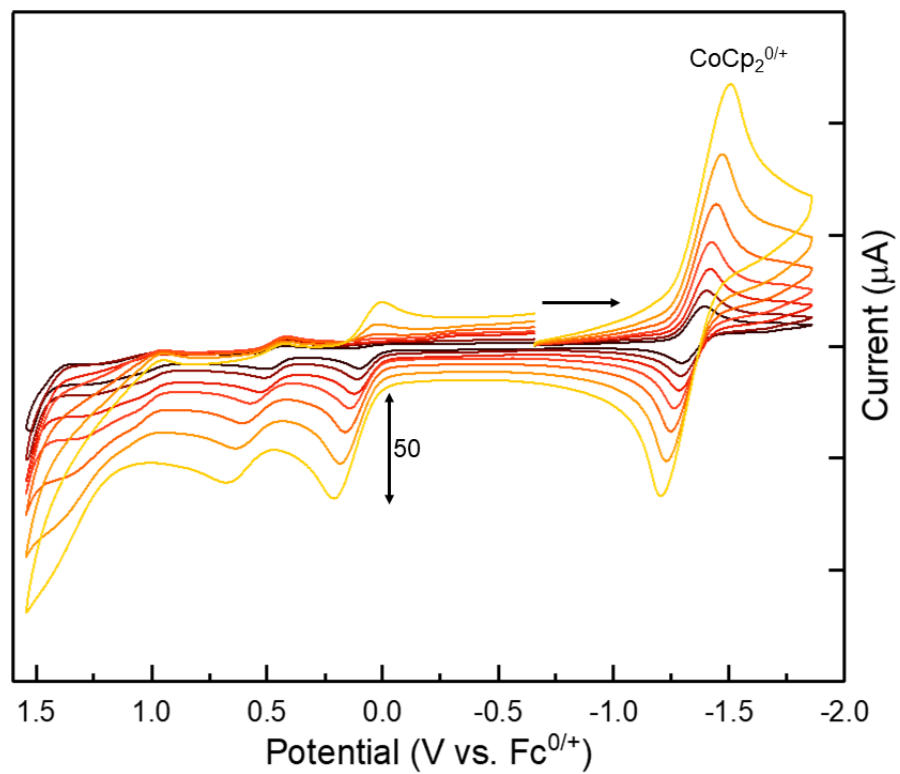


Figure S63. Cyclic voltammetry of **2** (2.0 mM) showing the scan rate dependence from 25-1600 mV/s. Arrows show sweep origin and current scale

References

- [1] a) W. A. King, X.-L. Luo, B. L. Scott, G. J. Kubas, K. W. Zilm, *J. Am. Chem. Soc.* **1996**, *118*, 6782-6783; b) W. A. King, B. L. Scott, J. Eckert, G. J. Kubas, *Inorg. Chem.* **1999**, *38*, 1069-1084; c) K. D. Welch, W. G. Dougherty, W. S. Kassel, D. L. DuBois, R. M. Bullock, *Organometallics* **2010**, *29*, 4532-4540; d) E. B. Hulley, K. D. Welch, A. M. Appel, D. L. DuBois, R. M. Bullock, *J. Am. Chem. Soc.* **2013**, *135*, 11736-11739; e) E. B. Hulley, M. L. Helm, R. M. Bullock, *Chem. Sci.* **2014**, *5*, 4729-4741; f) R. H. Reimann, E. Singleton, *J. Organomet. Chem.* **1972**, *38*, 113-119; g) R. J. LeSuer, C. Buttolph, W. E. Geiger, *Anal. Chem.* **2004**, *76*, 6395-6401.
- [2] a) M. M. Francl, W. J. Pietro, W. J. Hehre, J. S. Binkley, M. S. Gordon, D. J. Defrees, J. A. Pople, *J. Chem. Phys.* **1982**, *77*, 3654-3665; b) W. J. Hehre, Ditchfie.R, J. A. Pople, *J. Chem. Phys.* **1972**, *56*, 2257-2261.
- [3] M. Dolg, U. Wedig, H. Stoll, H. Preuss, *J. Chem. Phys.* **1987**, *86*, 866-872.
- [4] S. Grimme, *Chem. Eur. J.* **2012**, *18*, 9955-9964.
- [5] a) S. Grimme, J. Antony, S. Ehrlich, H. Krieg, *J. Chem. Phys.* **2010**, *132*, 154104; b) S. Grimme, S. Ehrlich, L. Goerigk, *J. Comp. Chem.* **2011**, *32*, 1456-1465.
- [6] A. V. Marenich, C. J. Cramer, D. G. Truhlar, *J. Phys. Chem. B* **2009**, *113*, 6378-6396.
- [7] F. Neese, *Wiley Interdiscip. Rev. Comput. Mol. Sci.* **2017**, *8*, e1327.
- [8] a) P. Bhattacharya, Z. M. Heiden, E. S. Wiedner, S. Raugei, N. A. Piro, W. S. Kassel, R. M. Bullock, M. T. Mock, *J. Am. Chem. Soc.* **2017**, *139*, 2916-2919; b) P. Bhattacharya, Z. M. Heiden, G. M. Chambers, S. I. Johnson, R. M. Bullock, M. T. Mock, *Angew. Chem. Int. Ed.* **2019**, 10.1002/anie.201903221; c) S. I. Johnson, S. P. Heins, C. M. Klug, E. S. Wiedner, R. M. Bullock, S. Raugei, *Chem. Commun.* **2019**, *55*, 5083-5086.
- [9] Bruker APEX2 (Version 2.1-4), SAINT (version 7.34A), SADABS (version 2007/4), BrukerAXS Inc, Madison, Wisconsin, USA. **2007**.
- [10] G. M. Sheldrick, *Acta Cryst.* **2015** A71, 3-8.
- [11] a) A. Altomare, C. Burla, M. Camalli, G. L. Casciarano, C. Giacovazzo, A. Guagliardi, A. G. G. Moliterni, G. Polidori, R. Spagna, *J. Appl. Cryst.* **1999**, *32*, 115-119. b) Altomare A, Casciarano G L, Giacovazzo C, Guagliardi A. *J. Appl. Cryst.* **1993**, *26*, 343-350.
- [12] a) G. M. Sheldrick (1997) SHELXL-97, University of Göttingen, Germany. b) Sheldrick GM. *Acta Cryst.* **2015**, C71, 3-8. b) S. Mackay, C. Edwards, A. Henderson, C. Gilmore, N. Stewart, K. Shankland, A. Donald, **1997**. University of Glasgow, Scotland.
- [13] D. Waasmaier, A. Kirfel, *Acta Cryst. A.* **1995**, *51*, 416-430.
- [14] L. J. Farrugia, *J. Appl. Cryst.* **1997** *30*, 565.
- [15] (a) A. Spek, *J. Appl. Cryst.* **2003**, *36*, 7-13; (b) P. van der Sluis, A. L. Spek, *Acta Cryst.* **1990**, A46, 194-201. (c) A. L. Spek. *Acta. Cryst.* **2009**, D65, 148-155.